Geosci. Model Dev. Discuss., doi:10.5194/gmd-2016-184, 2016
Manuscript under review for journal Geosci. Model Dev.
Published: 2 August 2016

Geoscientific Model Development Discussions Open Access EGU

Global 7-km mesh nonhydrostatic Model Intercomparison Project for improving TYphoon forecast (TYMIP-G7): Experimental design and preliminary results

Masuo Nakano[1], Akiyoshi Wada[2], Masahiro Sawada[2], Hiromasa Yoshimura[2], Ryo Onishi[1], Shintaro Kawahara[1], Wataru Sasaki[1], Tomoe Nasuno[1], Munehiko Yamaguchi[2], Takeshi Iriguchi[2], Masato Sugi[2], and Yoshiaki Takeuchi[2]

[1]Japan Agency for Marine-Earth Science and Technology, 3173-25 Showa-machi, Kanazawa-ku, Yokohama, Kanagawa 236-0001, Japan
[2]Meteorological Research Institute, Japan Meteorological Agency, 1-1 Nagamine, Tsukuba, Ibaraki 305-0052, Japan

Correspondence to: Masuo Nakano (masuo@jamstec.go.jp)

Abstract. Recent advances in high-performance computers facilitate operational numerical weather prediction by global hydrostatic atmospheric models with horizontal resolution ~10 km. Given further advances in such computers and the fact that the hydrostatic balance approximation becomes invalid for spatial scales < 10 km, development of global nonhydrostatic models with high accuracy is urgently needed.

The Global 7-km mesh nonhydrostatic Model Intercomparison Project for improving TYphoon forecast (TYMIP-G7) is designed to understand and statistically quantify the advantage of high-resolution nonhydrostatic global atmospheric models for improvement of tropical cyclone (TC) prediction. The 137 sets of 5-day simulations using three next-generation nonhydrostatic global models with horizontal resolution 7 km, and conventional hydrostatic global model with horizontal resolution 20 km are run on the Earth Simulator. The three 7-km mesh nonhydrostatic models are the nonhydrostatic global spectral atmospheric Model using Double Fourier Series (DFSM), Multi-Scale Simulator for the Geoenvironment (MSSG), and Nonhydrostatic ICosahedral Atmospheric Model (NICAM). The 20-km mesh hydrostatic model is the operational Global Spectral Model (GSM) of the Japan Meteorological Agency.

Compared with the 20-km mesh GSM, the 7-km mesh models reduce systematic errors of TC track and intensity predictions but still have difficulties in predicting rapid TC intensification. The benefits of the multi-model ensemble method are confirmed to be valid for the 7-km mesh nonhydrostatic global models. Whereas the three 7-km mesh models reproduce a typical axisymmetric mean inner-core structure such as primary and secondary circulations, simulated TC structures and their intensity in each case are very different among the models. Moreover, the simulated track is not always better than that of the 20-km mesh GSM. These results suggest that development of more sophisticated initialization techniques and model physics is needed for further improvement of TC prediction.

1 Introduction

1.1 Global model

A global model is a major tool for providing fundamental information to operational weather forecasting at daily, weekly, and seasonal time scales. Moreover, such models provide initial and lateral boundary conditions to limited-area models, which furnish fundamental information to local-scale weather forecasts. Therefore, operational numerical weather prediction centres have been developing sophisticated global models with high resolution and accuracy. Because such models require huge computational resources, their development strongly depends on advances in high-performance computers. Recent computer progress has facilitated reasonable operation of global models with horizontal resolution ~10 km. Indeed, the European Centre for Medium-Range Weather Forecasts (ECMWF) has operated a global model with horizontal resolution 9 km since March 2016. Therefore, sooner or later, it is expected that all numerical weather prediction centres will operate global models with horizontal grid intervals less than 10 km.

Developing high-resolution models with horizontal grid spacing < 10 km must resolve three challenges. The first is to use a nonhydrostatic equation system. In the Earth's atmosphere, hydrostatic balance is established for spatial scales larger than 10 km, with high accuracy. Therefore, the primitive equation system, which approximates the vertical momentum equation with the hydrostatic balance equation, has been used in conventional global models. The second challenge is to use a dynamical core that effectively runs on state-of-the-art, massive parallel computer systems. Many conventional global models use the spectral method in which the Legendre transform is used for meridional expansion of certain prognostic variables. Because the computational cost of this transform increases with the third power of the number of grid points and communication costs become great, one of the solutions is to avoid that transform. The last challenge is to implement sophisticated physical schemes suitable for high-resolution models, especially for clouds, because they can be partially resolved in the model with horizontal resolution 10 km.

Because developing operational numerical weather prediction models with high accuracy requires huge computational and human resources, the concept of the transition of research to operations (R2O) has been encouraged recently. For example, the Hurricane Weather Research and Forecasting Model (Bernardet et al., 2015) and an atmosphere–ocean coupled limited-area model (Ito et al., 2015) have been developed based on R2O in the United States and Japan, respectively. In Japan, two next-generation, nonhydrostatic global atmospheric models have already been developed and used in research community. These are called the Multi-Scale Simulator for the Geoenvironment (MSSG) and Nonhydrostatic ICosahedral Atmospheric Model (NICAM). In addition, the Meteorological Research Institute (MRI) of the Japan Meteorological Agency (JMA) has developed a next-generation nonhydrostatic atmospheric model called the nonhydrostatic global spectral atmospheric Model using Double Fourier Series (DFSM). To gain knowledge to develop and improve nonhydrostatic global models and share them with the research and operational communities are one of the aims of the present study.

1.2 TC forecasts

Tropical cyclones (TCs) are characterized by violent winds and torrential rain. These cause tremendous damage to human lives, property, and socioeconomic activity via landslides, floods, and storm surge. Since approximately 26 TCs (more than 30% of the global average) form on annual average in the western North Pacific, accurate TC track and intensity forecast is of great concern to East Asian countries for mitigating the impacts of associated disasters. The JMA has primary responsibility for TC forecasts in the western North Pacific as a Regional Specialized Meteorological Centre (RSMC) of the World Meteorological Organization. The agency has operated a 20-km mesh global atmospheric model for predicting weather and TC track and intensity since 2007. Therefore, upgrading their global atmospheric model is a promising approach to improve TC forecasts in the western North Pacific.

Errors in track prediction of the JMA operational global atmospheric model have been decreased on average by half over the past 20 years (JMA, 2014), as the operational model has been upgraded. For example, TC track prediction error in a 30-hour forecast with a 60-km mesh global model was ~200 km in 1997, decreasing to ~100 km in 2010 with a 20-km mesh model. Although we have continuously striven to improve TC track prediction, there are still abnormally large track prediction errors called "forecast busts" (e.g., Carr and Elsberry, 2000). Typhoons Conson (2004) (Yamaguchi et al., 2009) and Fengshen (2008) (Yamada et al., 2016) are typical examples. Predicted tracks by tens-of-km mesh global models for Fengshen showed serious poleward-bias recurving to far from the Philippine Islands, but the typhoon made landfall in the Philippines according to best-track analyses (Joint Typhoon Warning Center, 2008). Yamada et al. (2016) reported that a 3.5-km mesh, next-generation nonhydrostatic global model successfully simulated its landfall in the Philippines. Increase in

Geosci. Model Dev. Discuss., doi:10.5194/gmd-2016-184, 2016
Manuscript under review for journal Geosci. Model Dev.
Published: 2 August 2016

Geoscientific Model Development Discussions

the horizontal resolution of global atmospheric models with appropriate physical schemes can potentially reduce bust cases and annual mean errors of TC track prediction.

Despite the advances in TC track prediction, improvement of TC intensity predictions by global atmospheric models remains a challenge. One of the factors that impede improvement of intensity prediction is a lack of horizontal resolution to capture essential mechanisms of TC intensity change. TC intensity and its variation are closely related to the inner-core structure and convective activity (e.g., Rogers et al., 2013; Wang and Wang, 2014). Recent studies using a high-resolution, limited-area atmospheric model show that use of horizontal resolution of a few kilometres is necessary to realistically reproduce the inner-core structure and associated convection (e.g. Braun and Tao, 2000; Gentry and Lackmann, 2010; Kanada and Wada, 2015). Fierro et al. (2009) examined the dependence of TC intensity prediction using horizontal resolutions from 30 to 1 km, pointing out that predicted TC intensity become rapidly realistic with resolutions between 15 and 5 km. Therefore, use of a high-resolution global atmospheric model with horizontal resolution < 10 km is promising to improve TC intensity and track prediction.

1.3 TYMIP-G7

The main objectives of the "Global 7-km mesh nonhydrostatic Model Intercomparison Project for improving TYphoon forecast" (TYMIP-G7) are to understand and statistically quantify the advantage of high-resolution global atmospheric models toward improvement of TC track and intensity forecasts. The project is conducted as a strategic program of the Earth Simulator of the Japan Agency for Marine-Earth Science and Technology (JAMSTEC). We accomplish the objective by model intercomparison of three 7-km mesh nonhydrostatic atmospheric models (DFSM, MSSG, and NICAM) and a 20-km mesh hydrostatic operational atmospheric model of JMA (Global Spectral Model; GSM) in various cases. Because a huge amount of data are produced by each model, we develop an effective method to handle and visualize those data. Sharing the knowledge obtained in this project among research and operational communities would facilitate R2O.

This paper consists of six sections. Section 2 describes the common experimental design, including the cases and output dataset. Section 3 briefly overviews the scientific outcomes of each model and describes detailed specifications. Section 4 presents the analysis method and visualization. Preliminary results regarding the advantage of high-resolution models in TC prediction and simulated TC structure are presented in Sect. 5. Section 6 is devoted to conclusions and future work.

2 Experimental design

We imitated JMA operational specifications to conduct 5-day numerical experiments with the models (DFSM, GSM, MSSG and NICAM). JMA 6-hourly global objective analysis data were used for each model to derive atmospheric initial conditions. The data were provided based on the GSM grid system, a linear Gaussian grid with horizontal resolution 20 km and hybrid sigma-pressure vertical coordinate. DFSM and GSM interpolated data directly to their model grids, whereas MSSG and NICAM preliminarily interpolated the data into common latitude/longitude grids and pressure levels and then interpolated to their model grids. A merged satellite and in situ data global daily sea surface temperature (SST) product with horizontal resolution 0.25° (Kurihara et al., 2006) was used for oceanic initial conditions of SST and sea ice concentration. Because an atmospheric model was used in the present study, SSTs for 5-day integration should be given as boundary conditions. It was assumed that an SST anomaly from observed daily climatology on an initial date persisted during the 5-day period. Although no diurnal cyclone of SST was input to the models, NICAM can simulate the diurnal cycle because it is coupled with a simple bulk ocean model, as described later.

The project was implemented using the Earth Simulator, a supercomputer system operated by the JAMSTEC. The Earth Simulator is based on NEC SX-ACE, a distributed-memory, massively parallel vector system with a total of 5,120 computational nodes. Each node has one central processing unit, which consists of four processing cores, and 64 GB main memory. Theoretical peak performance of the entire system is 1.3 peta floating-point operations per second.

2.1 Cases

We conducted the project for two stages: from June 2015 to September 2015 and from October 2015 to March 2016. The first stage addressed TCs from September to October in 2013 when the season was the most activate TC season since 1951. We could calculate nine TCs in 52 runs (Table 1). However, we detected some flaws in MSSG and NICAM so that we could not perform some of the numerical experiments. The second stage addressed a lifecycle of a TC such as genesis, rapid intensification, recurvature, extratropical transition in addition to Madden–Julian Oscillation (MJO; Madden and Julian, 1972) and Boreal summer intraseasonal oscillation (BSISO; Wang and Rui, 1990; Wang and Xie, 1997). After we improve the flaws, we examined 13 TCs in 85 runs (Table 2) in addition to the numerical experiments in the first stage.

2.2 Dataset

Model output data every 1 or 3 hours from each experiment (Tables 1 and 2) were stored for analyses. Components of the output are listed in Table 3. Although each model uses its own grid system, the output data were prepared for a regular latitude/longitude (lat/lon) grid system. In TYMIP-G7, we used GrADS file formats (set of 4-byte IEEE 754 floating-point standard with big endian binary file, and control files in text format) that are common in atmospheric and oceanic research fields. The domain of the output data covers the globe, including the western North Pacific Ocean (100–180°E, 0°–60°N). For MJO and BSISO cases (20 runs, see Table 1 and 2), it also covers the Tropics (30°E–100°W, 15°S–30°N). Horizontal resolution of the global dataset is 1.25°. The data for the western North Pacific Ocean and the Tropics are prepared with horizontal resolution ~0.07° (7 km) by DFSM, MSSG and NICAM and ~0.19° (20 km) by GSM. In the vertical, the data were prepared on 32 common pressure levels (1000, 975, 950, 925, 900, 875, 850, 825, 800, 775, 750, 700, 650, 600, 550, 500, 450, 400, 350, 300, 250, 225, 200, 175, 150, 125, 100, 70, 50, 30, 20, and 10 hPa).

3 Models

We use three 7-km mesh nonhydrostatic global atmospheric models in TYMIP-G7 (Fig. 1). The DFSM has been developed in the MRI of JMA. The MSSG has been developed at the JAMSTEC. The NICAM has been developed at the JAMSTEC, The University of Tokyo, and RIKEN Advanced Institute for Computational Science. In addition, we use the GSM with horizontal grid spacing ~20 km to quantify the advantage of higher-resolution models. The DFSM and GSM are spectral models and MSSG and NICAM are grid models. The following subsection details the aforementioned models (Table 4) and experimental design.

3.1 GSM and DFSM

The GSM is a hydrostatic global spectral atmospheric model using spherical harmonics. The JMA has used it operationally to provide fundamental information for forecasts. The model was put into operation in 1988 with resolution T63L16 (200-km mesh), where “Tx” refers to a horizontal triangular spectral truncation with total wavenumber x, using a quadratic Gaussian grid, and “Ly” refers to the number of vertical layers y. Resolution of the operational GSM increased to T106L21 (120-km mesh) in 1989, T213L30 (60-km mesh) in 1996, T213L40 in 2001, TL319L40 (60-km mesh) in 2005, TL959L60 (20-km mesh) in 2007, and TL959L100 in 2014 (JMA, 2016), where “TLx” refers to a horizontal triangular spectral truncation with total wavenumber x, using a linear Gaussian grid (Hortal, 2002).

The JMA has also used the GSM as the principal part of an ensemble prediction system for medium-range weather forecasts. The forecast data were widely provided via the framework of The observing-system research and predictability

Geosci. Model Dev. Discuss., doi:10.5194/gmd-2016-184, 2016
Manuscript under review for journal Geosci. Model Dev.
Published: 2 August 2016

experiment Interactive Grand Global Ensemble (TIGGE) for the research community. TIGGE data have been used for various applications, including TC track prediction (Yamaguchi et al., 2012, 2015) and the MJO (Matsueda and Endo, 2011). In addition, the GSM has been used for producing atmospheric reanalysis datasets, i.e., the Japanese 25-year ReAnalysis (JRA-25; Onogi et al., 2007) and Japanese 55-year ReAnalysis (JRA-55; Kobayashi et al., 2015). MRI global climate models have been developed based on the GSM and have been used in climate research such as global warming projections and stratospheric study (e.g. Shibata et al., 1999; Mizuta et al., 2006; Yukimoto et al., 2011). TC activity in a future climate has been intensively studied using various model physics and horizontal resolutions (Murakami and Sugi, 2010; Murakami et al., 2012a, b).

The MRI developed DFSM by changing the hydrostatic dynamical core of the GSM using spherical harmonics to a nonhydrostatic dynamical core using double Fourier series expansion (Yoshimura, 2012). The DFSM uses the same basis functions of double Fourier series as Cheong (2000). In the DFSM, fast Fourier transform is used instead of Legendre transform in the meridional direction. Because computational cost of the Fast Fourier transform is much smaller than that of Legendre transform, especially for high resolution, DFSM is applicable to finer resolution. DFSM gives nearly the same results as the GSM using Legendre transform; comparison of 2-day forecasts using the 60-km resolution model was shown by Yoshimura and Matsumura (2005).

In the GSM and DFSM, a two-time-level, semi-implicit, semi-Lagrangian scheme (e.g., Hortal, 2002) is used to facilitate a long time step for computational efficiency. The vertically conservative semi-Lagrangian scheme is used in advection calculation (Yoshimura and Matsumura, 2003; Yoshimura and Matsumura, 2005; Yukimoto et al., 2011), and a correction method similar to that described by Priestley (1993) and Gravel and Staniforth (1994) is used for global conservation in material transport. To save computational cost, we used a reduced grid (Miyamoto, 2006) in which the number of zonal grid points is decreased, especially at high latitudes (Fig. 1).

Because the DFSM resolution is ~7 km (ML2559L100; "MLx" refers to a horizontal truncation with zonal wavenumber x, using spectral truncation based on a linear equally-spaced latitude grid), the model applies the nonhydrostatic option, which essentially uses the same nonhydrostatic equations as in the ALADIN-NH nonhydrostatic limited-area spectral model (Bubnová et al., 1995; Bénard et al., 2010) and nonhydrostatic version of the Integrated Forecast System global model of ECMWF (Wedi and Smolarkiewicz, 2009). However, there are some differences in the method of integration. The DFSM uses a non-constant coefficient semi-implicit scheme. The preconditioned Generalized Conjugate Residual method, a fast-converging iteration method, is used to solve simultaneous linear equations in the semi-implicit scheme of the DFSM (Yoshimura, 2012). Recalculation is necessary only for the non-constant linear terms during the iteration. It is found that only a single iteration is sufficient for convergence.

Physical packages included in the GSM and DFSM are the same as in the March 2014 version of the operational global atmospheric model of the JMA. A prognostic cumulus parameterization scheme (Randall and Pan, 1993) and other schemes in the GSM are used in the DFSM, without any changes. The physical process is described in detail in JMA (2013).

3.2 MSSG

The MSSG is an atmosphere-ocean coupled nonhydrostatic model aimed at seamless simulation from global to local scales (Takahashi et al., 2006, 2013). The MSSG consists of atmospheric (MSSG-A) and ocean (MSSG-O) components. The MSSG uses a conventional lat/lon grid system for regional simulations and the Yin-Yang grid system (Kageyama and Sato, 2004; Baba et al., 2010), which consists of two overlapping lat/lon grids that avoid the polar singularity problem for global simulations. The MSSG has been used in a wide range of applications. A global atmosphere-ocean coupled experiment at 11-km horizontal resolution with nested region of 2.7-km horizontal resolution simulated sea surface cooling caused by a TC along its track (Takahashi et al., 2013). High-resolution regional atmospheric simulations have been conducted to investigate the influence of choice of cloud microphysics scheme and in-cloud turbulence on cloud

Geosci. Model Dev. Discuss., doi:10.5194/gmd-2016-184, 2016
Manuscript under review for journal Geosci. Model Dev.
Published: 2 August 2016

Geoscientific Model Development Discussions Open Access EGU

development (Onishi et al., 2011, 2012). MSSG-O with 2-km horizontal resolution has been used to investigate the dispersion of radionuclides released from the Fukushima Dai-ichi nuclear power plant (Choi et al., 2013) and the effect of wind on long-term summer water temperature trends in Tokyo Bay, Japan at 200-m horizontal resolution (Lu et al., 2015). MSSG-A with 5-m spatial resolution has been used in building-resolving urban atmosphere simulations to clarify heat environments of streets (Takahashi et al., 2013).

In the present study, MSSG-A is mainly used. Its dynamical core is based on the nonhydrostatic equations, and predicts the three wind components, air density, and pressure. Each horizontal computational domain covers 4056 × 1352 grids in the Yin-Yang lat/lon grid system. Average horizontal grid spacing is 7 km. The vertical level consists of 55 vertical layers at the top height of 40 km with the lowermost vertical layer at 75 m. The third-order Runge–Kutta scheme is used for time integration. The fast terms related to acoustic and gravity waves are calculated separately, with a shorter time step (Wicker and Skamarock, 2002). A fifth-order upwind scheme (Wicker and Skamarock, 2002) was chosen for momentum advection and the second-order weighted average flux scheme with the Superbee flux limiter (Toro, 1989) for scalar advection. For turbulent diffusion, the Mellor–Yamada–Nakanishi–Niino level 2.5 scheme (Nakanishi and Niino, 2009) was used. The MSSG-Bulk model (Onishi and Takahashi, 2012), a six-category bulk cloud microphysics model, is used for explicit cloud physics. Model Simulation radiation TRaNsfer code version 10 (MstrnX; Sekiguchi and Nakajima, 2008) is used for calculating longwave and shortwave radiation transfer.

During the first stage of the project, an issue in which extraordinary increases in precipitable water appeared in the 5-day integrations when the conventional bulk surface flux model of Zhang and Anthes (1982) was used for both land and ocean surfaces. This issue was solved by use of the COARE 3.0 model (Fairall et al., 1996, 2003) for ocean surface fluxes, with Zhang and Anthes (1982) used only for land surface fluxes. This combination was used for all simulations in the second stage. It seems that the combination appeared to enhance MSSG prediction skill, judging from the fact that its TC track predictions were better on average than those of the GSM in the second stage, but poorer in the first stage.

3.3 NICAM

NICAM (Satoh et al., 2008, 2014) has been developed as a climate model and can explicitly resolve clouds without any convective parameterization, which is known for the most ambiguous component in a conventional climate model (Randall et al., 2003). From the first appearance of realistic cloud-resolving simulation using 3.5-km-mesh horizontal resolution by Miura et al. (2007a), NICAM has been mainly used for studying tropical meteorological systems, such as the MJO (Miura et al., 2007b, Nasuno, 2013; Miyakawa et al., 2014), TC genesis from the MJO in boreal winter (Fudeyasu et al., 2008, 2010a, 2010b), TC genesis from the BSISO in the western North Pacific (Oouchi et al., 2009; Nakano et al., 2015), and BSISO in the northern Indian Ocean (Taniguchi et al., 2010; Yanase et al., 2010). NICAM has also been used for quasi-real-time forecast systems during field observation campaigns to support field observation (Nasuno, 2013). Recent progress of high-performance computing infrastructure, such as the K-computer, a 10-petaflop supercomputer in Japan, facilitates 870-m mesh global simulation (Miyamoto et al., 2013, 2015; Kajikawa et al., 2016). This is the highest resolution to date (10 July 2016). Climate simulations (30-year) using a 14-km mesh model (Kodama et al., 2015) and large-member (10240 members) ensemble data assimilation based on an ensemble Kalman filter (Miyoshi et al., 2015) have also been executed.

NICAM uses the icosahedral grid system that covers the globe with almost uniform grid size, avoiding the polar singularity problem. Increased horizontal resolution is attained by recursively dividing horizontal grids in half. Therefore, the possible horizontal resolution is discrete and represented in "g-level," which means the number of divisions of a horizontal grid. In this project, the 2014 version of NICAM (called NICAM.14.3) is used with horizontal resolution of g-level 10, corresponding to a 7-km mesh. The vertical level consists of 38 vertical layers to a top height of 36.7 km, with the lowest layer at 80 m. NICAM uses a fully compressible nonhydrostatic equation system for dynamics of the atmosphere. The model uses an icosahedral grid system in the horizontal with the Arakawa A-grid and terrain-following coordinate with Lorenz grid in the vertical. The equations are discretized using the finite volume method in flux form. The numerical scheme guarantees conservation of total mass and energy. The second-order Runge–Kutta scheme is primarily used for time integration, but third-order Runge–Kutta is used for some cases to avoid computational instability. NICAM uses the split-explicit scheme, known as the horizontal explicit and vertical implicit scheme, to avoid restriction of the Courant–Friedrichs–Lewy condition for acoustic waves. The NICAM Single-moment Water 6 cloud microphysics scheme (Tomita, 2008) is used for cloud microphysics without any convective parameterization. Planetary boundary layer processes are calculated using the Mellor–Yamada–Nakanishi–Niino level 2 scheme (Nakanishi and Niino, 2004), implemented and examined by Noda et al. (2010). Longwave and shortwave radiation transfer is calculated using MstrnX (Sekiguchi and Nakajima, 2008). Land surface processes are computed by Minimal Advanced Treatments of Surface Interaction and Runoff (MATSIRO; Takata et al., 2003). NICAM is coupled with a simple slab ocean model of 15-m depth to simulate a diurnal cycle of SST. The calculated SST is nudged with a persistent SST anomaly with e-folding time of 7 days. Surface flux is calculated by the Louis (1979) scheme, with sea surface roughness length parameterization by Moon et al. (2007).

During the first stage of this project, there was a frequent problem of division by zero in MATSIRO that was never experienced in the simulations with coarser horizontal resolution. This issue was fixed before simulations in the second stage, and abnormal cases in the first stage were recalculated. It was confirmed that this fix had a slight impact on the prediction results.

3.4 Computer performance on the Earth Simulator

Computational performance is one of the metrics to decide on an operational numerical weather forecast model. Table 5 summarizes computational performances of DFSM, MSSG, NICAM and GSM. Execution efficiency for each model on the Earth Simulator is 15%–17%, except for DFSM. GSM used the same model physics as DFSM, but its execution efficiency is higher than that of DFSM. This is mainly because calculation of the Legendre transform, done only in the GSM, is very substantial, but its execution efficiency is excellent. DFSM was optimized for the Earth Simulator in the project and become about four times faster than before, but there may be room for further optimization. Among the 7-km mesh models, DFSM requires the least computational resources, particularly in node-hours. This is largely because of the relatively long time step (Table 3), owing to the semi-implicit semi-Lagrangian scheme within that model. More sophisticated cloud microphysics schemes in MSSG and NICAM than that in DFSM is also a factor in increased computational cost of the first two models. MSSG requires the greatest computational resource, about twice that of NICAM, even though both models used the conventional advection schemes. The difference in node-hours between MSSG and NICAM are mainly attributable to the difference in vertical resolutions and number of vertical levels, which are sensitive to the time step setting.

4 Analysis methods and visualization

4.1 TC tracking

We extract TC tracking in each experiment using hourly mean sea level pressure (SLP) data with horizontal resolution ~7 km for DFSM, MSSG and NICAM, and 20 km for GSM. A TC centre is defined as a minimum SLP point from the predicted mean SLP field smoothed 100 times by a 1-2-1 filter, for each longitude and latitude. The initial TC centre is defined within a radius of 1° from a centre position based on RSMC Tokyo best-track data. The next centre position is defined as the minimum SLP point from the smoothed mean SLP field within a radius of 1° from the previous centre position. The tracking terminates when the minimum SLP points reach a proximity of 1° from the lateral boundary in the domain of the output data.

Geosci. Model Dev. Discuss., doi:10.5194/gmd-2016-184, 2016
Manuscript under review for journal Geosci. Model Dev.
Published: 2 August 2016

4.2 Multi-model ensemble mean

The multi-model ensemble mean (MME) is applied to the three 7-km mesh models (DFSM, MSSG, and NICAM). MME is a simple ensemble average derived from a combination of individual models, which reduces average forecast errors relative to the best individual predictions by individual models. MME also provides additional information on forecast uncertainty, enhancing forecast confidence (Goerss, 2000; Yamaguchi et al., 2012).

4.3 Visualization

To compare the numerical experiment results among the four models visually and simultaneously, we have developed a Web application that allows the display of multiple visualization results simultaneously. Figure 2 shows a screen capture of this application, which portrays digital globes using Cesium.js (Analytical Graphics, Inc., 2015), a WebGL-based virtual globe and map engine. Visualization results of each model are overlaid on them. We used Volume Data Visualizer for Google Earth (VDVGE; Kawahara, 2012; Kawahara, 2015) to depict visualization results for overlaying. VDVGE is a visualization software that exports visualization results coded in KML, a data format suitable for Google Earth. Furthermore, we added a function to VDVGE for exporting visualization results in CZML, a data format suitable for Cesium.js. In the Web application, a user is able to view the animation display with time-series visualization results of each model, while changing the three-dimensional viewpoint synchronously. Each model result is displayed selectively using buttons on top of the screen. The application enables easy comparison of numerical experiments among the four models.

5 Results

5.1 Track predictions

To quantify the advantages of high resolution on TC track prediction, we examined time series of errors of TC track prediction with reference to the RSMC Tokyo best track. The samples used for verification are common to each model in both the first and second stages. We perform verification for each first and second stage separately because of differences in model settings (described in Sect. 2) when an atmospheric disturbance reached at least tropical depression strength.

In the first stage, TC track prediction by DFSM and NICAM showed better performance after forecast times (FTs) of 36 h and 96 h, respectively, relative to the prediction of GSM. Track errors in MSSG were larger than those of GSM. Adjustment of the surface flux scheme, which was done in the second stage to solve a precipitable water issue, may have reduced track errors in MSSG. Figure 3 addresses time series in the second stage. TC track predictions by DFSM, MSSG and NICAM have better performance than does GSM. However, the reduction in track error depends on the TC case. That is, the use of finer resolution alone does not always improve TC track prediction. This suggests that improvement of the initial condition and of physical processes in each model are also important to improve track prediction.

We also validated MME using track predictions of the three models with reference to RSMC Tokyo best-track data. MME track prediction gives the smallest track errors for FT = 84–120 h. The reduction rate of position error from MME is ~24% at FT = 120 h relative to that of GSM. Position error of MME at that FT corresponds to that of GSM at FT = 102 h. The relatively favourable performance of MME appeared at medium-range time scales (FT = 84–120 h) as compared with the performance of individual model runs, consistent with the findings of Yamaguchi et al. (2012). Although MME has a promising result in improving TC track prediction, future work is required to achieve more robust results and answer scientific and practical questions, such as in which cases is MME effective and why.

5.2 Intensity predictions

Figure 4 shows time series of the average central pressure and standard deviations for each model relative to RSMC Tokyo best-track data for the first and second stages. The central pressure in DFSM, MSSG and NICAM show relatively

Geosci. Model Dev. Discuss., doi:10.5194/gmd-2016-184, 2016
Manuscript under review for journal Geosci. Model Dev.
Published: 2 August 2016

Geoscientific Model Development Discussions Open Access

small bias compared with the error in GSM. Thus, global 7-km mesh models help decrease systematic positive errors in central pressure. At least, the comparison between GSM and DFSM results suggests that a high-resolution model reduces systematic bias in TC intensity prediction, because both those models have the same specification except for horizontal resolution. This improvement is attributed to reduction of TC track forecast error (~100 km at FT = 120 h; Fig. 3) and better representation of TC structures, as shown in the next subsection. The GSM shows gradual growth of positive bias, whereas the 7-km mesh models show intensity error decrease by FT = 24 h. After this initial decrease, the errors begin to grow in model-specific ways. MSSG and NICAM shows gradual growth of positive bias by FT = 84 h and the error become saturated, whereas DFSM has gradual growth of negative bias by FT = 120 h. Noticeably, MME shows almost no bias after FT = 24 h. This demonstrates the advantage of MME for TC intensity and track prediction.

To evaluate characteristics of TC intensity prediction for each model, we show scatter diagrams of the relationship between predicted and RSMC Tokyo best-track central pressures (Fig. 5). First, GSM could not generally reproduce a central pressure lower than 940 hPa. DFSM sometimes reproduces a central pressure lower than 910 hPa, although such a TC frequently over-intensified after FT = 72 h. One of the reasons for such excessive intensification is the use of the same physical schemes tuned for a 20-km mesh model as that in the GSM. Through sensitivity experiments on the cumulus parameterization and cloud scheme, we confirmed that a modified physical scheme suitable to DFSM with 7-km horizontal resolution decreased the over-intensification (not shown). MSSG and NICAM reproduce a central pressure of nearly 930 hPa with relatively small standard deviation relative to the best-track data. From the standpoint of intensification rate, however, MSSG and NICAM still predicted rapid deepening of central pressure with difficulty, particularly the initiation of intensification.

5.3 Predictions of TC structure

Figure 6 shows horizontal distributions of hourly precipitation overlaid on SLP for Typhoon Wipha at 14 October 2013, 06:00:00 UTC (FT = 96 h) initiated at 10 October 2013, 06:00:00 UTC as an example. At that time, RSMC Tokyo best-track data showed that central pressure, maximum wind speed, and radius of surface wind speeds of 25 m s^{-1} (R25) were 940 hPa, 80 knot (40 m s^{-1}), and 120 nautical miles (220 km), respectively. Satellite observation (Fig. 7) suggests that convection in the inner core had an asymmetric structure and was most active in the northeastern semicircle, with spiral rain bands. GSM simulates a very weak TC (980 hPa), with maximum surface wind speed smaller than 25 m s^{-1} and a weak and disorganized precipitation pattern compared with those from DFSM, MSSG, and NICAM. DFSM has the most intense (897 hPa) and compact eyewall structure among the three 7-km mesh models, with R25 of ~95 km. In addition, the TC predicted by DFSM has double eyewalls. The difference of precipitation and SLP patterns between GSM and DFSM is attributed to their contrasting horizontal resolutions, because both models use the same configuration and specifications except for horizontal resolution. MSSG and NICAM simulate intensities (934 and 953 hPa, respectively) and R25 values (approximately 265 and 175 km axisymmetric means, respectively) similar to RSMC best-track analyses. However, precipitation patterns are completely different. MSSG shows a concentric eyewall, represented by a well-organized circular precipitation pattern. The horizontal scale of the eyewall is wider than that of the DFSM. NICAM predicts a band-shape precipitation pattern, indicating that the simulated TC does not establish a concentric eyewall as in DFSM and MSSG. Even though both MSSG and NICAM use explicit microphysical schemes without any cumulus parameterization, there are significant differences in the simulated TC structures.

Composite analyses of a radial-height section were done for Typhoon Wipha at the time of maximum intensity during its lifetime, using the results of 15 experiments (Table 1). Figure 8 shows radius-height cross sections of azimuthal mean radial and tangential wind speeds. DFSM realistically reproduces the secondary circulation of a typical TC, represented by inflow toward the TC centre in the lower troposphere and outflow in the upper troposphere, compared with the secondary circulation of the GSM. However, the axisymmetric structure predicted by DFSM differs greatly from that by

MSSG and NICAM. The simulated inflow layer in MSSG is the thickest among the three models, more than double that of DFSM. Another unique structure from MSSG is inflow just below the upper outflow layer. The TC vortex height in NICAM is shallower than that of DFSM and MSSG. For example, the maximum height of tangential wind speed = 15 m s^{-1} is ~100 hPa for DFSM and MSSG but 170 hPa for NICAM. The radius of maximum winds (RMW) in NICAM is more than twice that of DFSM. The slope of RMW simulated by NICAM is larger than that of DFSM and MSSG. Even though the horizontal resolution of the models is identical, differences in specifications such as dynamics and physical processes yields substantial differences in TC inner core structure.

Figure 9 shows the relationship between maximum axisymmetric mean tangential wind speed and RMW. X-marks show averages within bins every 5 m s^{-1}. The GSM is unable to reproduce the RMW derived from extended best-track data (mean or median RMWs are 64.6 and 55.5 km; Kimball and Mulekar, 2004), because the predicted RMW is > 100 km. Skamarock (2004) stated that seven times the horizontal grid spacing is the scale of the finest resolvable modes, which corresponds to ~140 km for GSM. Thus, it is difficult to reproduce an RMW < 100 km. The resolvable scale of the 7-km mesh model is ~50 km. MSSG and NICAM are able to reproduce the reduction in RMW with TC intensification, with a mean simulated RMW > 50 km. The reduction in RMW is consistent with observation by aircraft penetration (e.g., Fig. 12 of Stern et al., 2015). The RMW predicted by DFSM is the smallest among the four models. We need sensitivity studies to clarify which factors cause the RMW differences, which are closely related to differences in vertical structure of the inner core (Fig. 8).

6 Conclusions and future work

The TYMIP-G7 project have been implemented in two stages, from June 2015 through March 2016. The aim of the project is to statistically quantify and understand the advantage of high-resolution, global atmospheric models toward the improvement of 5-day TC track and intensity forecasts. We performed numerical experiments for many TC cases in 137 runs using three 7-km mesh global nonhydrostatic atmospheric models. These were the DFSM, MSSG, and NICAM. We also included the 20-km mesh global hydrostatic atmospheric model, GSM, on the Earth Simulator of JAMSTEC. We statistically evaluated errors of TC track and intensity predictions, with the following main results.

(C1) The 7-km models statistically improve both TC intensity and track predictions, whereas improvement of individual TC track depended on the case.

(C2) The MME is a promising approach to further enhancement of TC intensity and track predictions.

(C3) Predicting rapid intensification is still challenging for 7-km mesh global atmospheric models.

(C4) Predicted TC structure differs greatly among the three models, even though they have the same horizontal resolution.

To follow up the above results toward further improvement of TC prediction, we must answer the following questions:

(Q1) Why are the TC predictions improved by high-resolution models?

(Q2) What causes the differences in simulated TC structure among the three 7-km mesh atmospheric global models, such as radius of maximum winds, eyewall slope, inflow and outflow layers, and rainbands?

To answer (Q1), intercomparison of forecasts by the 20-km mesh GSM and 7-km mesh models (DFSM, MSSG, and NICAM) is the first step. Concerning (Q2), the predicted TC structure depends on physics schemes, such as cloud microphysics, planetary boundary layer, and surface flux, as well as the dynamical core of the model. To understand the impacts of the model physics schemes, sensitivity experiments are needed, e.g., altering those schemes and/or tuning parameters.

In addition, the following topics are suggested for future work:

(F1) Extended-range forecasts, contributing to TC genesis and MJO/BSISO forecasts;

(F2) Atmosphere-ocean coupled experiments to examine impacts on TC intensity and track and MJO/BSISO;

(F3) Further high-resolution experiments to study impacts of better inner-core representation on TC intensity and track; and

(F4) Data assimilation to contribute to model validation and understanding of TC processes and model initialization.

These topics are addressed below.

An advantage of global models for TC prediction over limited-area models is coverage of multiscale atmospheric phenomena, from a mesoscale vortex to synoptic environments. Because TC genesis strongly depends on synoptic environments modulated by the MJO/BSISO, global models should be used for its forecasting. Indeed, Nakano et al. (2015) and Xiang et al. (2015) showed that TC genesis is predictable up to 2 weeks in advance; this great skill in TC genesis forecasting was attributed to strong skill in BSISO/MJO forecasting. We are conducting extended-range (longer than 2 weeks) forecast experiments using four models in several cases, and will investigate the advantage of high-resolution modes.

In the present project, atmosphere models have been used thus far. However, studies have shown that atmosphere-ocean coupled processes are essential for especially slow-moving, intense TCs. These processes affect TC structure and thereby track and intensity. In addition, an atmosphere-ocean coupled model is more skilful for MJO/BSISO forecasts. MSSG is already capable of coupling MSSG-A with MSSG-O. Also, NICAM has been coupled with the Center for Climate System Research Ocean COmponent Model (COCO; Hasumi, 2006). Therefore, we will use these coupled global models to examine the impacts of global atmosphere-ocean processes on TC forecasts.

To improve the high-resolution models, validation of simulated phenomena using observations is essential. Understanding of essential processes and modelling thus require high-resolution spatiotemporal observation. Recent advances in satellite observations furnish quantitatively and qualitatively rich observational data. However, the spatiotemporal resolution is still insufficient for validation of TC structure simulated by high-resolution models. Aggressively developing data assimilation techniques using satellite observations (e.g., Zhang et al., 2016, Okamoto et al., 2016) is a promising means of obtaining high-resolution, spatiotemporal, three-dimensional TC structure, including the cloud convection scale (~O(1 km)). In addition, applying such cloud-resolving analysis to deriving initial conditions of high-resolution models may improve TC prediction.

Data availability

The initial and boundary data for the models and model outputs are available under collaborative framework between MRI, JAMSTEC, and related institute or university.

Acknowledgements

This project was conducted as “The Earth Simulator Strategic Project with Special Support” of JAMSTEC. All numerical experiments were run on the Earth Simulator (NEC SX-ACE). The study was partly supported by HPCI Strategic Programs for Innovative Research (SPIRE) Field 3, FLAGSHIP 2020 project of the Ministry of Education, Culture, Sports, Science and Technology (MEXT), and KAKENHI 26282111, 26400475, 15K05292 of the Japan Society for the Promotion of Science (JSPS). The authors thank Ms. Mikiko Ikeda, Mr. Yuichi Saitoh, and Mr. Hiromitsu Fuchigami for supporting the experiments on the Earth Simulator. The authors also acknowledge Mr. Hideaki Kawai and Mr. Eiki Shindo for fruitful discussions. The schematic diagram of the NICAM grid was provided by Professor Masaki Satoh.

References

Analytical Graphics, Inc.: Cesium, http://cesiumjs.org, (accessed 8 Jul. 2016), 2015.

Arakawa, T., Yoshimura, H., Saito, F., and Ogochi, K.: Data exchange algorithm and software design of KAKUSHIN coupler Jcup, Procedia Comput. Sci., 4, 1516–1525, 2011.

Baba, Y., Takahashi, K., Sugimura, T., and Goto, K.: Dynamical core of an atmospheric general circulation model on a yin–yang grid. Mon. Wea. Rev., 138, 3988–4005, 2010.

Bénard, P., Vivoda, J., Mašek, J., Smolíková, P., Yessad, K., Smith, Ch., Brožková, R. and Geleyn, J.-F.: Dynamical kernel of the Aladin-NH spectral limited-area model: Revised formulation and sensitivity experiments. Quart. J. Roy. Meteor. Soc., 136, 155-169, 2010.

Bernardet, L., Tallapragada, V., Bao, S., Trahan, S., Kwon, Y., Liu, Q., Tong, M., Biswas, M., Brown, T., Stark, D., Carson, L., Yablonsky, R., Uhlhorn, E., Gopalakrishnan, S., Zhang, X., Marchok, T., Kuo, B., and Gall, R.: Community Support and Transition of Research to Operations for the Hurricane Weather Research and Forecasting Model, Bull. Amer. Meteor. Soc., 96, 953-960, doi: 10.1175/BAMS-D-13-00093.1, 2015.

Braun, S. A., and Tao, W.-K.: Sensitivity of high-resolution simulations of Hurricane Bob (1991) to planetary boundary layer parameterizations, Mon. Wea. Rev., 128, 3941–3961, 2000.

Bubnová, R., Hello, G., Bénard, P., and Geleyn, J.-F.: Integration of the fully elastic equations cast in the hydrostatic pressure terrain-following coordinate in the framework of the ARPEGE/Aladin NWP system. Mon. Wea. Rev., 123, 515-535, 1995.

Carr III, L. E., and Elsberry, R. L.: Dynamical tropical cyclone track forecast errors. Part I: Tropical region error sources. Wea. Forecast., 15, 641-661, doi: 10.1175/1520-0434(2000)015<0641:DTCTFE>2.0.CO;2, 2000.

Cheong, H.-B.: Application of double Fourier series to the shallow-water equations on a sphere. J. Comput. Phy., 165, 261-287, 2000.

Choi, Y., Kida, S. and Takahashi, K., The impact of oceanic circulation and phase transfer on the dispersion of radionuclides released from the Fukushima Dai-ichi Nuclear Power Plant, Biogeosci., 10, 4911-4925, doi:10.5194/bg-10-4911-2013, 2013.

Fairall, C.W., Bradley, E.F., Rogers, D.P., Edson, J.B., and Young, G.S., Bulk parameterization of air-sea fluxes for Tropical Ocean-Global Atmosphere Coupled-Ocean Atmosphere Response Experiment, J. Geophys. Res., 101, 747-3764, 1996.

Fairall, C. W., Bradley, E. F., Hare, J.E., Grachev, A. A. and Edson, J. B.: Bulk Parameterization of Air-Sea Fluxes: Updates and Verification for the COARE Algorithm, J. Clim., 16, 571-591, 2003.

Fierro, A. O., Rogers, R. F., Marks, F. D., and Nolan, D. S.: The Impact of Horizontal Grid Spacing on the Microphysical and Kinematic Structures of Strong Tropical Cyclones Simulated with the WRF-ARW Model, Mon. Wea. Rev. 137, 3717-3743, doi: 10.1175/2009MWR2946.1, 2009

Fudeyasu, H., Wang, Y., Satoh, M., Nasuno, T., Miura, H., and Yanase, W.: Global cloud-system-resolving model NICAM successfully simulated the lifecycles of two real tropical cyclones, Geophys. Res. Lett., 35, doi: 10.1029/2008GL036003, 2008.

Fudeyasu, H., Wang, Y., Satoh, M., Nasuno, T., Miura, H., and Yanase, W.: Multiscale Interactions in the Life Cycle of a Tropical Cyclone Simulated in a Global Cloud-System-Resolving Model. Part I: Large-Scale and Storm-Scale Evolutions. Mon. Wea. Rev., 138, 4285-4304, doi: 10.1175/2010MWR3474.1, 2010a.

Fudeyasu, H., Wang, Y., Satoh, M., Nasuno, T., Miura, H., and Yanase, W.: Multiscale Interactions in the Life Cycle of a Tropical Cyclone Simulated in a Global Cloud-System-Resolving Model. Part II: System-Scale and Mesoscale Processes*. Mon. Wea. Rev., 138, 4305-4327, doi: 10.1175/2010MWR3475.1, 2010b.

Gentry, M. S., and Lackmann, G. M.: Sensitivity of simulated tropical cyclone structure and intensity to horizontal resolution, Mon. Wea. Rev., 138, 688–704, doi: 10.1175/2009MWR2976.1, 2010.

Goerss, J. S.: Tropical Cyclone Track Forecasts Using an Ensemble of Dynamical Models. Mon. Wea. Rev., 128, 1187–1193, doi:10.1175/1520-0493(2000)128<1187:TCTFUA>2.0.CO;2., 2000.

Gravel, S. and Staniforth, A.: A mass-conserving semi-Lagraingian scheme for the shallow-water equations. Mon. Wea. Rev., 122, 243-248, 1994.

Hasumi, H.: CCSR Ocean Component Model (COCO) version 4.0. CCSR Rep 25. The University of Tokyo, Chiba, Japan, 2006.

Hortal, M.: The development and testing of a new two-time-level semi-Lagrangian scheme (SETTLS) in the ECMWF forecast model. Q. J. R. Meteor. Soc., 128, 1671-1687, doi: 10.1002/qj.200212858314, 2002.

Ito, K., Kuroda, T., Saito, K. and Wada, A.: Forecasting a Large Number of Tropical Cyclone Intensities around Japan Using a High-Resolution Atmosphere–Ocean Coupled Model, Wea. and Forecast., 30, 793-808, doi: 10.1175/WAF-D-14-00034.1, 2015.

Japan Meteorological Agency: Outline of the operational numerical weather prediction at the Japan Meteorological Agency. Appendix to WMO technical progress report on the global data-processing and forecasting system and numerical weather prediction,188p.http://www.jma.go.jp/jma/jma-eng/jma-center/nwp/outline2013-nwp/index.htm, 2013.

Japan Meteorological Agency: Annual Report on the Activities of the RSMC Tokyo -Typhoon Center, 90p, http://www.jma.go.jp/jma/jma-eng/jma-center/rsmc-hp-pub-eg/AnnualReport/2014/Text/Text2014.pdf, 2014.

Japan Meteorological Agency: The Upgrade History of the Global Spectral Model. http://www.wis-jma.go.jp/ddb/latest_modelupgrade.txt, 2016.

Joint Typhoon Warning Center: 2008 Annual Tropical Cyclone Report, 116p, http://www.usno.navy.mil/NOOC/nmfc-ph/RSS/jtwc/atcr/2008atcr.pdf

Kageyama, A. and Sato, T.: The Yin-Yang Grid: An Overset Grid in Spherical Geometry. Geochem. Geophys.Geosyst., 5, Q09005, doi:10.1029/2004GC000734, 2004.

Kajikawa, Y., Miyamoto, Y., Yoshida, R., Yamaura, T., Yashiro, H. and Tomita, H.: Resolution dependence of deep convections in a global simulation from over 10-kilometer to sub-kilometer grid spacing, Prog. Earth Planet. Sci., 3, 16, doi:10.1186/s40645-016-0094-5, 2016

Kanada, S. and Wada, A.: Numerical study on the extremely rapid intensification of an intense tropical cyclone, Typhoon Ida (1958). J. Atmos. Sci., 72, 4194–4217. doi: 10.2151/jmsj.2015-037, 2015.

Kawahara, S., Onishi, R., Goto, K. and Takahashi, K., Realistic Representation of Clouds in Google Earth, Proc. SIGGRAPH Asia 2015 VHPC, Doi: 10.1145/2818517.2818541, 2015.

Kawahara, S.: VDVGE, http://www.jamstec.go.jp/ceist/aeird/avcrg/vdvge.en.html, (accessed 27 April. 2016), 2012.

Kimball, S. K., and Mulekar, M. S.: A 15-year climatology of North Atlantic tropical cyclones. Part I: Size parameters. J. Clim., 17, 3555–3575, 2004.

Kobayashi, S., Ota, Y., Harada, Y., Ebita, A., Moriya, M., Onoda, H., Onogi, K, Kamahori, H., Kobayashi, C., Endo, H., Miyaoka, K. and Takahashi, K.: The JRA-55 Reanalysis: General Specifications and Basic Characteristics, J. Meteor. Soc. Jpn., 93, 5-48, doi: 10.2151/jmsj.2015-001, 2015

Kodama, C., Yamada, Y., Noda, A. T., Kikuchi, K., Kajikawa, Y., Nasuno, T., Tomita, T., Yamaura, T., Takahashi, T. G., Hara, M., Kawatani, Y., Satoh, M. and Sugi, M.: A 20-year climatology of a NICAM AMIP-type simulation. J. Meteor. Soc. Japan, 93, 393-424, doi:10.2151/jmsj.2015-024, 2015.

Kurihara, Y., Sakurai, T. and Kuragano, T.: Global daily sea surface temperature analysis using data from satellite microwave radiometer, satellite infrared radiometer and in-situ observations (in Japanese), Weather Bull., 73, s1–s18, 2006.

Louis, J. F.: A parametric model of vertical eddy fluxes in the atmosphere, Bound.-Layer Meteor., 2, 187-202, 1979.

Louis, J. F., Tiedtke, M., and Geleyn, J. F.: A short history of the operational PBL parameterization at ECMWF. Proc. Workshop on Planetary Boundary Layer Parameterization, Reading, United Kingdom, ECMWF, 59–79, 1982.

Lu, L.-F., Onishi, R. and Takahashi, K.: The effect of wind on long-term summer water temperature trends in Tokyo Bay, Japan, Ocean Dyn., 65, 919-930, 2015.

Madden, R. A. and Julian, P. R.: Description of Global-Scale Circulation Cells in the Tropics with a 40–50 Day Period, J. Atmos. Sci., 29, 1109-1123, 1972.

Matsueda, M. and Endo, H.: Verification of medium-range MJO forecasts with TIGGE. Geophys. Res. Lett., 38, L11801, doi:10.1029/2011GL047480, 2011.

Mellor, G. L. and Yamada, T.: A hierarchy of turbulence closure models for planetary boundary layers. J. Atmos. Sci., 31, 1791–1806, 1974.

Mellor, G. L. and Yamada, T.: Development of a turbulence closure model for geophysical fluid problems. Rev. Geophys. Space Phys., 20, 851–875, 1982.

Miller, M. J., Palmer, T. N., and Swinbank, R.: Parameterization and influence of subgridscale orography in general circulation and numerical weather prediction models, Meteor. Atmos. Phys., 40, 84-109, 1989.

Miura, H., Satoh, M., Tomita H., Noda, A. T., Nasuno, T., and Iga, S.: A short-duration global cloud-resolving simulation with a realistic land and sea distribution, Geophys. Res. Lett., 34, L02804, doi:10.1029/2006GL027448, 2007a.

Miura, H., Satoh, M., Nasuno T., Noda, A. T., and Oouchi, K.: A Madden-Julian oscillation event realistically simulated by a global cloud-resolving model, Science, 318, 1763–1765, doi:10.1126/science.1148443, 2007b.

Miyakawa, T., Satoh, M., Miura, H., Tomita, H., Yashiro, H., Noda, A. T., Yamada, Y., Kodama, C., Kimoto, M., and Yoneyama, K.: Madden-Julian oscillation prediction skill of a new-generation global model demonstrated using a supercomputer. Nat Comm., 5: 3769. doi:10.1038/ncomms4769, 2014.

Miyamoto, K.: Introduction of the Reduced Gaussian Grid into the Operational Global NWP model at JMA. CAS/JSC WGNE Research Activities in Atmospheric and Ocean Modelling, 36, 6.9-6.10, 2006.

Miyamoto, Y., Kajikawa, Y., Yoshida, R., Yamaura, T., Yashiro, H., and Tomita, H.: Deep moist atmospheric convection in a subkilometer global simulation, Geophys. Res. Lett., 40, 4922–4926, doi:10.1002/grl.50944, 2013.

Miyamoto, Y., Yoshida, R., Yamaura T., Yashiro H., Tomita H., and Kajikawa Y.: Does convection vary in different cloud disturbances?, Atmos. Sci. Lett., 2015.

Miyoshi T., Kondo, K., and Terasaki, K.: Big Ensemble Data Assimilation in Numerical Weather Prediction, Computer, 48, 15–21; doi:10.1109/MC.2015.332, 2015.

Mizuta, R., Oouchi, K., Yoshimura, H., Noda, A, Katayama, K., Yukimoto, S., Hosaka, M., Kusunoki, S., Kawai, H., and Nakagawa, M.: 20-km-mesh global climate simulations using JMA-GSM model -- mean climate states. J. Meteor. Soc. Japan, 84, 165-185, doi:10.2151/jmsj.84.165, 2006.

Moon, I.-J., Ginis, I., Hara, T., and Thomas B.: A Physics-Based Parameterization of Air–Sea Momentum Flux at High Wind Speeds and Its Impact on Hurricane Intensity Predictions, Mon. Wea. Rev., 135, 2869-2878, 2007.

Murakami, H. and Sugi, M.: Effect of model resolution on tropical cyclone climate projections. SOLA, 6, 73-76, doi: 10.2151/sola.2010-019, 2010.

Murakami, H., Mizuta, R., and Shindo, E.: Future changes in tropical cyclone activity projected by multi-physics and multi-SST ensemble experiments using the 60-km-mesh MRI-AGCM. Clim. Dyn., 39, 2569-2584, doi: 10.1007/s00382-011-1223-x, 2012a.

Murakami, H., Wang, Y., Yoshimura, H., Mizuta, R., Sugi, M., Shindo, E., Adachi,Y., Yukimoto, S., Hosaka, M., Kusunoki, S., Ose, T., and Kitoh, A.: Future changes in tropical cyclone activity projected by the new high-resolution MRI-AGCM. J. Clim., 25, 3237-3260, doi: 10.1175/JCLI-D-11-00415.1, 2012b.

Nakanishi, M. and Niino, H.: An improved Mellor-Yamada level-3 model with condensation physics: Its design and verification. Bound.-Layer Meteor., 112, 1–31, 2004.

Nakanishi, M. and Niino, H.: An improved Mellor-Yamada level-3 model: Its numerical stability and application to a regional prediction of advection fog. Bound.-Layer Meteor., 119, 397–407, 2006.

Nakanishi, M. and Niino, H.: Development of an Improved Turbulence Closure Model for the Atmospheric Boundary Layer. J. Meteor. Soc. Japan, 87, 895–912, doi: 10.2151/jmsj.87.895, 2009.

Nakano, M., Nasuno, T., Sawada, M., and Satoh, M.: Intraseasonal variability and tropical cyclogenesis in the western North Pacific simulated by a global nonhydrostatic atmospheric model. Geophysical Research Letters, 42, 565-571, doi: 10.1002/2014GL062479, 2015.

Nasuno, T.: Forecast skill of Madden–Julian oscillation events in a global nonhydrostatic model during the CINDY2011/DYNAMO observation period. SOLA, 9, 69–73, doi: 10.2151/sola.2013-016, 2013.

Noda, A. T., Oouchi, K., Satoh, M., Tomita, H., Iga, S.-I., and Tsushima, Y.: Importance of the subgrid-scale turbulent moist process: Cloud distribution in global cloud-resolving simulations, Atmos Res., 96, 208–217, doi:10.1016/j.atmosres.2009.05.007, 2010.

Okamoto, K., Aonashi, K., Kubota, T., and Tashima, T.: Experimental assimilation of the GPM-Core DPR reflectivity profiles for Typhoon Halong (2014), Mon. Wea. Rev., doi: 10.1175/MWR-D-15-0399.1, 2016

Onishi, R., Takahashi, K. and Komori, S.: High-resolution simulations for turbulent clouds developing over the ocean. Gas Transfer at Water Surfaces (ed. S. Komori, W. McGillis & R. Kurose), Kyoto University Press, 6, 582–592, 2011.

Onishi, R. and Takahashi, K.: A warm-bin–cold-bulk hybrid cloud microphysical model. J. Atmos. Sci., 69, 1474–1497. doi: 10.1175/JAS-D-11-0166.1, 2012.

Onogi, K., Tsutsui, J., Koide, H., Sakamoto, M., Kobayashi, S., Hatsushika, H., Matsumoto, T., Yamazaki, N., Kamahori, H., Takahashi, K., Kadokura, S., Wada, K., Kato, K., Oyama, R., Ose, T., Mannoji, N., and Taira, R.: The JRA-25 Reanalysis, J. Meteor. Soc. Jpn., 85, 369-432, doi: 10.2151/jmsj.85.369, 2007

Oouchi, K., Noda, A. T., Satoh, M., Miura, H., Tomita, H., Nasuno,T., Iga, S.: A simulated preconditioning of typhoon genesis controlled by a boreal summer Madden-Julian Oscillation event in a global cloud-resolving mode.SOLA, 5, 65-68, doi: doi:10.2151/sola.2009-017, 2009.

Priestley, A.: A quasi-conservative version of the semi-Lagrangian advection scheme. Mon. Wea. Rev., 121, 621-629, 1993.

Randall, D. and Pan, D.-M.: Implementation of the Arakawa-Schubert cumulus parameterization with a prognostic closure. The representation of cumulus convection in numerical models, AMS Meteor. Monogr. Series, 46, 137–144, 1993.

Randall, D., Khairoutdinov, M., Arakawa, A., and Grabowski, W.: Breaking the Cloud Parameterization Deadlock. Bull. Amer. Meteorol. Soc., 84, 1547–1564, doi: 10.1175/BAMS-84-11-1547, 2003.

Rogers, R. F., Reasor, P. and Lorsolo, S.: Airborne doppler observations of the inner-core structural differences between intensifying and steady-state tropical cyclones. Mon. Wea. Rev., 141, 2970-2991, 2013.

Peng, X., Xiao, F. and Takahashi, K.: Conservation constraint for quasi-uniform overset grid on sphere. Quart. J. Roy. Meteor. Soc., 132, pp.979–996, 2006.

Satoh, M., Matsuno, T., Tomita, H., Miura, H., Nasuno, T. and Iga, S.: Nonhydrostatic icosahedral atmospheric model (NICAM) for global cloud resolving simulations. J. Comput. Phys., 227, 3486-3514, 2008.

Satoh, M., Tomita, H., Yashiro, H., Miura, H, Kodama, C., Seiki, T., Noda, A. T., Yamada, Y., Goto, D., Sawada, M., Miyoshi, T., Niwa, Y., Hara, M., Ohno, T., Iga, S., Arakawa, T., Inoue, T. and Kubokawa, H.: The non-hydrostatic icosahedral atmospheric model: description and development. Progress in Earth and Planetary Science, 1:18, 2014.

Sekiguchi, M. and Nakajima, T.: A k-distribution-based radiation code and its computational optimization for an atmospheric general circulation model. J. Quant. Spectrosc. Radiat. Transfer, 109, 2779-2793, 2008.

Shibata, K., Yoshimura, H., Ohizumi, M., Hosaka, M. and Sugi, M.: A simulation of troposphere, stratosphere and mesosphere with MRI/JMA98 GCM. Pap. Meteor. Geophys., 50(1), 15-53, 1999.

Skamarock, W. C.: Evaluating mesoscale NWP models using kinetic energy spectra. Mon. Wea. Rev., 132, 3019–3032, doi:10.1175/MWR2830.1, 2004.

Smith, R. N. B.: A scheme for predicting layer clouds and their water content in a general circulation model. Quart. J. Roy. Meteor. Soc., 116, 435–460, 1990.

Stern, D. P., Vigh, J. L., Nolan, D. S., and Zhang, F.: Revisiting the Relationship Between Eyewall Contraction and Intensification. J. Atmos. Sci., 72, 1283–1306, doi:10.1175/JAS-D-14-0261.1, 2015.

Takahashi, K., Peng, X., Ohnishi, R., Sugimura, T., Ohdaira, M., Goto, K. and Fuchigami, H.: Multi-Scale Weather/Climate Simulations with Multi-Scale Simulator for the Geoenvironment (MSSG) on the Earth Simulator. Ann. Rep. Earth Simulator Center, April 2006–March 2007, pp.27–33, ISSN 1348–5822, 2006.

Takahashi K., Onishi R., Baba Y., Kida S., Matsuda K., Goto, K. and Fuchigami, H.: Challenge toward the prediction of typhoon behaviour and down pour. J. Phys.: Conference Series 454:012,072, 2013.

Toro, E. F.: A weighted average flux method for hyperbolic conservation laws. Proc. Roy. Soc. London, A423, 401–418, 1989.

Takata, K, Emori, S., and Watanabe, T.: Development of the minimal advanced treatments of surface interaction and runoff. Global and Planet. Change, 38, 209-222, 2003.

Taniguchi, H., Yanase, W., and Satoh, M.: Ensemble Simulation of Cyclone Nargis by a Global Cloud-System-Resolving Model—Modulation of Cyclogenesis by the Madden-Julian Oscillation, J. Meteor. Soc. Jpn., 88, 571-591, doi: 10.2151/jmsj.2010-317, 2010.

Tomita, H.: New microphysical schemes with five and six categories by diagnostic generation of cloud ice, J. Meteorol. Soc. Japan, 86A, 121-142. doi: 10.2151/jmsj.86A.121, 2008.

Wang, B., and Rui, H.: Synoptic climatology of transient tropical intraseasonal convection anomalies: 1975–1985, Meteorol. Atmos. Phys., 44, 43–61, 1990.

Wang, B., and Xie, X.: A model for the boreal summer intraseasonal oscillation, J. Atmos. Sci., 54, 72–86, 1997.

Wang, H., and Wang, Y.: A numerical study of typhoon Megi (2010): Part I: Rapid intensification. Mon. Wea. Rev., 142, 29-48, doi:10.1175/MWR-D-13-00070.1, 2014.

Wedi, N. P. and Smolarkiewicz, P. K.: A framework for testing global non-hydrostatic models. Q. J. R. Meteor. Soc., 135, 469-484, doi: 10.1002/qj.377, 2009.

Wicker, L. J. and Skamarock, W.C.: Time-split-ting methods for elastic models using forward time schemes, Monthly Weather Review, 130, 2088–2097, 2002.

Xiang, B., Lin, S.-J., Zhao, M., Zhang, S., Vecchi, G., Li, T., Jiang, X., Harris, L., and Chen, J.-H.: Beyond weather time-scale prediction for hurricane Sandy and super typhoon Haiyan in a global climate model. Mon. Wea. Rev., 143, 524-535, doi: 10.1175/MWR-D-14-00227.1, 2015.

Yabu, S.: Development of longwave radiation scheme with consideration of scattering by clouds in JMA global model, CAS/JSC WGNE Research Activities in Atmospheric and Oceanic Modelling. 43. 4.07-4.08, 2013.

Yamada H, Nasuno T, Yanase W, and Satoh M: Role of the vertical structure of a simulated tropical cyclone in its motion: A case study of Typhoon Fengshen (2008), SOLA, accepted, 2016.

Yamaguchi, M., Iriguchi, T., Nakazawa, T., and Wu, C.-C.: An observing system experiment for Typhoon Conson (2004) using a singular vector method and DOTSTAR data. Mon. Wea. Rev., 137, 2801-2816, 2009.

Yamaguchi, M., Nakazawa, T. and Hoshino, S.: On the relative benefits of a multi-centre grand ensemble for tropical cyclone track prediction in the western North Pacific. Quart. J. Roy. Meteor. Soc., 138, 2019–2029, doi:10.1002/qj.1937, 2012.

Yamaguchi, M., Vitart, F., Lang, S. T. K., Magnusson, L., Elsberry, R. L., Elliott, G., Kyouda, M., and Nakazawa, T.: Global distribution on the skill of tropical cyclone activity forecasts from short- to medium-range time scales. Wea. Forecast, 30, 1695-1709, doi: 10.1175/WAF-D-14-00136.1, 2015.

Yanase, W., Taniguchi, H., and Satoh, M.: The genesis of tropical cyclone Nargis (2008): Environmental modulation and numerical predictability. J. Meteor. Soc. Japan, 88, 497-519, doi: 10.2151/jmsj.2010-314, 2010.

Yoshimura, H. and Matsumura, T.: A Semi-Lagrangian Scheme Conservative in the Vertical Direction. CAS/JSC WGNE Research Activities in Atmospheric and Ocean Modeling, 33, 3.19-3.20, 2003.

Yoshimura, H. and Matsumura, T.: A two-time-level vertically-conservative semi-Lagrangian semi-implicit double Fourier series AGCM. CAS/JSC WGNE Research Activities in Atmospheric and Ocean Modeling, 35, 3.25-3.26, 2005.

Yoshimura, H.: Development of a nonhydrostatic global spectral atmospheric model using double Fourier series. CAS/JSC WGNE Research Activities in Atmospheric and Ocean Modeling, 42, 3.05-3.06, 2012.

Yukimoto, S., and Coauthors: Meteorological Research Institute-Earth System Model Version 1 (MRI-ESM1) –Model Description–. Technical Reports of the Meteorological Research Institute, No. 64, 2011.

Zhang, D. and Anthes, R. A.: A high-resolution model of the planetary boundary layer—sensitivity tests and comparisons with SESAME-79 Data. J. Appl. Meteor., 21, 1594–1609, 1982.

Zhang, F., Minamide, M., and Clothiaux, E. E.: Potential impacts of assimilating all-sky infrared satellite radiances from GOES-R on convection-permitting analysis and prediction of tropical cyclones, Geophys. Res. Lett., 43, 2954–2963, doi:10.1002/2016GL068468, 2016.

Geosci. Model Dev. Discuss., doi:10.5194/gmd-2016-184, 2016
Manuscript under review for journal Geosci. Model Dev.
Published: 2 August 2016

Geoscientific Model Development Discussions

Table 1 List of initial times for stage 1 of TYMIP-G7

	Initial time	Typhoon case (*Italic*: weaker than Tropical Storm, ***Bold italic***: ***extratropical cyclone***)	DFSM	GSM	MSSG	NICAM
1	12 September 2013, 00:00:00 UTC	*Man-yi*	○	○	○	○
2	12 September 2013, 06:00:00 UTC	*Man-yi*	○	○	○	○
3	12 September 2013, 12:00:00 UTC	*Man-yi*	○	○	○	○
4	12 September 2013, 18:00:00 UTC	*Man-yi*	○	○	○	○
5	13 September 2013, 00:00:00 UTC	Man-yi	○	○	○	○
6	30 September 2013, 00:00:00 UTC	Wutip, Sepat, *Fitow*	○	○	○	○
7	30 September 2013, 06:00:00 UTC	Wutip, Sepat, *Fitow*	○	○	○	○(*1)
8	30 September 2013, 12:00:00 UTC	Wutip, Sepat, *Fitow*	○	○	○	○
9	30 September 2013, 18:00:00 UTC	Wutip, Sepat, *Fitow*	○	○	○	○
10	1 October 2013, 00:00:00 UTC	***Wutip***, Sepat, Fitow, *Danas*	○	○	○	○
11	1 October 2013, 06:00:00 UTC	Sepat, Fitow, *Danas*	○	○	○	○(*1)
12	1 October 2013, 12:00:00 UTC	Sepat, Fitow, *Danas*	○	○	○	○(*1)
13	1 October 2013, 18:00:00 UTC	Sepat, Fitow, *Danas*	○	○	○	○(*1)
14	2 October 2013, 00:00:00 UTC	Sepat, Fitow, *Danas*	○	○	○	○(*1)
15	2 October 2013, 06:00:00 UTC	Sepat, Fitow, *Danas*	○	○	○	○
16	2 October 2013, 12:00:00 UTC	Sepat, Fitow, *Danas*	○	○	○	○
17	2 October 2013, 18:00:00 UTC	***Sepat***, Fitow, *Danas*	○	○	○	○(*1)
18	3 October 2013, 00:00:00 UTC	***Sepat***, Fitow, *Danas*	○	○	○	○
19	3 October 2013, 06:00:00 UTC	***Sepat***, Fitow, *Danas*	○	○	○	○
20	3 October 2013, 12:00:00 UTC	***Sepat***, Fitow, *Danas*	○	○	○	○
21	3 October 2013, 18:00:00 UTC	***Sepat***, Fitow, *Danas*	○	○	○	○(*1)
22	4 October 2013, 00:00:00 UTC	Fitow, *Danas*	○	○	○	○(*1)
23	9 October 2013, 00:00:00 UTC	***Danas***,*Nari*,*Wipha*	○	○	○	○
24	9 October 2013, 06:00:00 UTC	***Danas***,*Nari*,*Wipha*	○	○	○	○
25	9 October 2013, 12:00:00 UTC	Nari,*Wipha*	○	○	○	○
26	9 October 2013, 18:00:00 UTC	Nari,*Wipha*	○	○	○	○
27	10 October 2013, 00:00:00 UTC	Nari,*Wipha*	○	○	○	○
28	10 October 2013, 06:00:00 UTC	Nari,*Wipha*	○	○	○	○
29	10 October 2013, 12:00:00 UTC	Nari,Wipha	○	○	○	○
30	10 October 2013, 18:00:00 UTC	Nari,Wipha	○	○	○	○
31	11 October 2013, 00:00:00 UTC	Nari,Wipha	○	○	○	○
32	11 October 2013, 06:00:00 UTC	Nari,Wipha	○	○	○	○
33	11 October 2013, 12:00:00 UTC	Nari,Wipha	○	○	○	○
34	11 October 2013, 18:00:00 UTC	Nari,Wipha	○	○	○	○
35	12 October 2013, 00:00:00 UTC	Nari,Wipha	○	○	○	○
36	12 October 2013, 06:00:00 UTC	Nari,Wipha	○	○	○	○
37	12 October 2013, 12:00:00 UTC	Nari,Wipha	○	○	○	○
38	17 October 2013, 12:00:00 UTC	***Wipha***, Francisco	○	○	○	○
39	17 October 2013, 18:00:00 UTC	***Wipha***, Francisco	○	○	○	○
40	18 October 2013, 00:00:00 UTC	***Wipha***, Francisco	○	○	○	○
41	18 October 2013, 06:00:00 UTC	***Wipha***, Francisco	○	○	○	○
42	18 October 2013, 12:00:00 UTC	***Wipha***, Francisco	○	○	○	○(*1)
43	18 October 2013, 18:00:00 UTC	Francisco	○	○	○	○

Geosci. Model Dev. Discuss., doi:10.5194/gmd-2016-184, 2016
Manuscript under review for journal Geosci. Model Dev.
Published: 2 August 2016

Geoscientific Model Development Discussions
Open Access
EGU

44	19 October 2013, 00:00:00 UTC	Francisco, *Lekima*	○	○	○	○(*1)
45	19 October 2013, 06:00:00 UTC	Francisco, *Lekima*	○	○	○	○
46	19 October 2013, 12:00:00 UTC	Francisco, *Lekima*	○	○	○	○
47	19 October 2013, 18:00:00 UTC	Francisco, *Lekima*	○	○	○	○
48	20 October 2013, 00:00:00 UTC	Francisco, *Lekima*	○	○	○	○
49	20 October 2013, 06:00:00 UTC	Francisco, *Lekima*	○	○	○	○
50	20 October 2013, 12:00:00 UTC	Francisco, *Lekima*	○	○	○	○(*1)
51	20 October 2013, 18:00:00 UTC	Francisco, *Lekima*	○	○	○	○
52	21 October 2013, 00:00:00 UTC	Francisco, *Lekima*	○	○	○	○

(*1): rerun with fixed version of MATSIRO (Sect. 2.2.3)

Geosci. Model Dev. Discuss., doi:10.5194/gmd-2016-184, 2016
Manuscript under review for journal Geosci. Model Dev.
Published: 2 August 2016

Geoscientific Model Development Discussions
Open Access
EGU

Table 2 Same as Table 1, but for stage 2

	Initial time	Typhoon case (*Italic*: weaker than Tropical Storm, ***Bold italic*: extratropical cyclone**) and MJO/BSISO case	DFSM	GSM	MSSG	NICAM(*2)
1	6 June 2013, 12:00:00 UTC	*Yagi*	○	○	○	○
2	7 June 2013, 00:00:00 UTC	*Yagi*	○	○	○	○
3	7 June 2013, 12:00:00 UTC	*Yagi*	○	○	○	○
4	8 June 2013, 00:00:00 UTC	*Yagi*	○	○	○	○
5	8 June 2013, 12:00:00 UTC	Yagi	○	○	○	○
6	9 June 2013, 00:00:00 UTC	Yagi	○	○	○	○
7	9 June 2013, 12:00:00 UTC	Yagi	○	○	○	○
8	10 June 2013, 00:00:00 UTC	Yagi	○	○	○	○
9	10 June 2013, 12:00:00 UTC	Yagi	○	○	○	○
10	11 June 2013, 00:00:00 UTC	Yagi	○	○	○	○
11	3 November 2013, 00:00:00 UTC	Krosa	○	○	○	○
12	3 November 2013, 12:00:00 UTC	Krosa, *Haiyan*	○	○	○	○
13	4 November 2013, 00:00:00 UTC	Krosa, Haiyan	○	○	○	○
14	4 November 2013, 12:00:00 UTC	***Krosa***, Haiyan	○	○	○	○
15	5 November 2013, 00:00:00 UTC	Haiyan	○	○	○	○
16	5 November 2013, 12:00:00 UTC	Haiyan	○	○	○	○
17	6 November 2013, 00:00:00 UTC	Haiyan	○	○	○	○
18	6 November 2013, 12:00:00 UTC	Haiyan	○	○	○	○
19	7 November 2013, 00:00:00 UTC	Haiyan	○	○	○	○
20	27 July 2014, 12:00:00 UTC	*Halong*	○	○	○	○
21	28 July 2014, 00:00:00 UTC	*Halong*	○	○	○	○
22	28 July 2014, 12:00:00 UTC	*Halong*, *Nakri*	○	○	○	○
23	29 July 2014, 00:00:00 UTC	Halong, *Nakri*	○	○	○	○
24	29 July 2014, 12:00:00 UTC	Halong, Nakri	○	○	○	○
25	30 July 2014, 00:00:00 UTC	Halong, Nakri	○	○	○	○
26	30 July 2014, 12:00:00 UTC	Halong, Nakri	○	○	○	○
27	31 July 2014, 00:00:00 UTC	Halong, Nakri	○	○	○	○
28	31 July 2014, 12:00:00 UTC	Halong, Nakri	○	○	○	○
29	1 August 2014, 00:00:00 UTC	Halong, Nakri	○	○	○	○
30	1 August 2014, 12:00:00 UTC	Halong, Nakri	○	○	○	○
31	2 August 2014, 00:00:00 UTC	Halong, Nakri	○	○	○	○
32	2 August 2014, 12:00:00 UTC	Halong, Nakri	○	○	○	○
33	3 August 2014, 00:00:00 UTC	Halong, Nakri	○	○	○	○
34	3 August 2014, 12:00:00 UTC	Halong, *Nakri*	○	○	○	○
35	4 August 2014, 00:00:00 UTC	Halong, *Nakri*	○	○	○	○
36	4 August 2014, 12:00:00 UTC	Halong	○	○	○	○
37	5 August 2014, 00:00:00 UTC	Halong	○	○	○	○
38	5 August 2014, 12:00:00 UTC	Halong	○	○	○	○
39	6 August 2014, 00:00:00 UTC	Halong	○	○	○	○
40	6 August 2014, 12:00:00 UTC	Halong	○	○	○	○
41	7 March 2015, 00:00:00 UTC	MJO	○	○	○	○
42	7 March 2015, 12:00:00 UTC	MJO	○	○	○	○
43	8 March 2015, 00:00:00 UTC	MJO	○	○	○	○
44	8 March 2015, 12:00:00 UTC	MJO	○	○	○	○
45	9 March 2015, 00:00:00 UTC	MJO	○	○	○	○
46	9 March 2015, 12:00:00 UTC	MJO, Pam	○	○	○	○
47	10 March 2015, 00:00:00 UTC	MJO, Pam	○	○	○	○
48	10 March 2015, 12:00:00 UTC	MJO, *Bavi*, Pam	○	○	○	○
49	11 March 2015, 00:00:00 UTC	MJO, *Bavi*, Pam	○	○	○	○
50	11 March 2015, 12:00:00 UTC	MJO, Bavi, Pam	○	○	○	○
51	27 June 2015, 00:00:00 UTC	BSISO	○	○	○	○
52	27 June 2015, 12:00:00 UTC	BSISO	○	○	○	○
53	28 June 2015, 00:00:00 UTC	BSISO	○	○	○	○
54	28 June 2015, 12:00:00 UTC	BSISO	○	○	○	○

Geosci. Model Dev. Discuss., doi:10.5194/gmd-2016-184, 2016
Manuscript under review for journal Geosci. Model Dev.
Published: 2 August 2016

55	29 June 2015, 00:00:00 UTC	BSISO	○	○	○	○
56	29 June 2015, 12:00:00 UTC	BSISO,*Chan-hom*	○	○	○	○
57	30 June 2015, 00:00:00 UTC	BSISO,*Chan-hom*	○	○	○	○
58	30 June 2015, 12:00:00 UTC	BSISO,Chan-hom	○	○	○	○
59	1 July 2015, 00:00:00 UTC	BSISO,Chan-hom	○	○	○	○
60	1 July 2015, 12:00:00 UTC	BSISO,Chan-hom	○	○	○	○
61	13 August 2015, 12:00:00 UTC		○	○	○	○
62	14 August 2015, 00:00:00 UTC	***Molave***, *Goni*, *Atsani*	○	○	○	○
63	14 August 2015, 12:00:00 UTC	***Molave***, *Goni*, *Atsani*	○	○	○	○
64	15 August 2015, 00:00:00 UTC	***Molave***, Goni, Atsani	○	○	○	○
65	15 August 2015, 12:00:00 UTC	***Molave***, Goni, Atsani	○	○	○	○
66	16 August 2015, 00:00:00 UTC	***Molave***, Goni, Atsani	○	○	○	○
67	16 August 2015, 12:00:00 UTC	***Molave***, Goni, Atsani	○	○	○	○
68	17 August 2015, 00:00:00 UTC	***Molave***, Goni, Atsani	○	○	○	○
69	17 August 2015, 12:00:00 UTC	***Molave***, Goni, Atsani	○	○	○	○
70	18 August 2015, 00:00:00 UTC	***Molave***, Goni, Atsani	○	○	○	○
71	18 August 2015, 12:00:00 UTC	Goni, Atsani	○	○	○	○
72	19 August 2015, 00:00:00 UTC	Goni, Atsani	○	○	○	○
73	19 August 2015, 12:00:00 UTC	Goni, Atsani	○	○	○	○
74	20 August 2015, 00:00:00 UTC	Goni, Atsani	○	○	○	○
75	20 August 2015, 12:00:00 UTC	Goni, Atsani	○	○	○	○
76	21 August 2015, 00:00:00 UTC	Goni, Atsani	○	○	○	○
77	6 September 2015, 00:00:00 UTC	Kilo, *Etau*	○	○	○	○
78	6 September 2015, 12:00:00 UTC	Kilo, *Etau*	○	○	○	○
79	7 September 2015, 00:00:00 UTC	Kilo, *Etau*	○	○	○	○
80	7 September 2015, 12:00:00 UTC	Kilo, Etau	○	○	○	○
81	8 September 2015, 00:00:00 UTC	Kilo, Etau	○	○	○	○
82	8 September 2015, 12:00:00 UTC	Kilo, Etau	○	○	○	○
83	9 September 2015, 00:00:00 UTC	Kilo, Etau	○	○	○	○
84	9 September 2015, 12:00:00 UTC	Kilo, ***Etau***	○	○	○	○
85	10 September 2015, 00:00:00 UTC	Kilo, ***Etau***	○	○	○	○

(*2): run with fixed version of MATSIRO (Sect. 2.2.3)

Geosci. Model Dev. Discuss., doi:10.5194/gmd-2016-184, 2016
Manuscript under review for journal Geosci. Model Dev.
Published: 2 August 2016

Geoscientific Model Development Discussions

Table 3 Output variables and domains

Domain	Interval	Variable	Horizontal resolution
Global	1 hour	Accumulated cloud ice (*cldi*), Accumulated cloud water (*cldw*), Outward longwave radiation (*olr*), Sea-level pressure (*psea*), 2-m specific humidity (*qs*), Sea surface temperature (*sst*), Total precipitable water (*tpw*), 2-m temperature (*ts*), 10-m zonal wind speed (*us*), 10-m meridional wind speed (*vs*)	1.25°
	1 hour (average)	Latent heat flux (*fllh*), Zonal wind stress (*flmu*), Meridional wind stress (*flmv*), Sensible heat flux (*flsh*), Precipitation (*prc*), Precipitation by cumulus parameterization (*prcc*)	1.25°
	3 hours	Cloud cover (*cvr*), Cloud water content (*cwc*), Cloud water (*qc* or *xc*), Cloud ice (*qi* or *xi*), rain water (*qr* or *xr*), snow (*qs* or *xs*), graupel (*qg* or *xg*), Specific humidity (*q*), Relative humidity (*rh*), Temperature (*t*), Zonal wind speed (*u*), Meridional wind speed (*v*), Vertical wind speed (*w*), Height (*z*)	1.25°
	3 hours (average)	Cumulus-induced heating (*hrcv*), Cloud-induced heating (*hrlc*), Radiation-induced heating (*hrr*), Turbulence-induced heating (*hrvd*), Cumulus-induced moistening (*qrcv*), Cloud-induced moistening (*qrlc*), Radiation-induced heating (*qrvd*), Cumulus-induced zonal acceleration (*urcv*), Turbulence-induced zonal acceleration (*urvd*), Cumulus-induced meridional acceleration (*vrcv*), Turbulence-induced meridional acceleration (*vrvd*)	1.25°
Western North Pacific/Tropics	1 hour	cldi, cldw, olr, psea, qs, sst, tpw, ts, us, vs	~7 km
	1 hour (average)	fllh, flmu, flmv, flsh, prc, prcc	~7 km
	3 hours	cvr, cwc, q, rh, t, u. v, w, z	~7 km
	3 hours (average)	hrcv, hrlc, hrr, hrvd, qrcv, qrlc, qrvd, urcv, urvd, vrcv, vrvd	~7 km

Geosci. Model Dev. Discuss., doi:10.5194/gmd-2016-184, 2016
Manuscript under review for journal Geosci. Model Dev.
Published: 2 August 2016

Geoscientific Model Development Discussions

Table 4 Brief description of specification for each global nonhydrostatic model

	DFSM	GSM	MSSG	NICAM
Horizontal resolution	7 km	20 km	7 km	7 km
Horizontal Grid configuration	Reduced linear equally-spaced latitude grid	Reduced linear Gaussian grid	Yin-yang grid	Icosahedral grid
Number of grids in horizontal direction	8845592	1312360	11184128	10485760
Vertical coordinate	Hybrid sigma-pressure coordinate	Hybrid sigma-pressure coordinate	Terrain-following coordinate	Terrain-following coordinate
Vertical levels	100 (top: 0.01 hPa, bottom: 999.0429 hPa(*3) (about 8m))	100 (top: 0.01 hPa, bottom: 999.0429 hPa(*3) (about 8m))	55 (top: 40 km, bottom: 75m)	38 (top: 36.7 km, bottom: 80 m)
Dynamical core	Nonhydrostatic spectral model using double Fourier series	Hydrostatic spectral model using spherical harmonics	Nonhydrostatic grid model using finite difference method	Nonhydrostatic grid model using finite volume method
Time step (s)	200	400	Variable	30
Cloud physics	Smith (1990)	Smith (1990)	Onishi & Takahashi (2012)	Tomita (2008)
Cumulus convection	Randall & Pan (1993)	Randall & Pan (1993)	Not used	Not used
Planetary boundary layer	MY2(Mellor & Yamada,1974,1982)	MY2 (Mellor & Yamada,1974,1982)	MYNN2.5 (Nakanishi & Niino, 2009)	MYNN2 (Nakanishi & Niino, 2004; Noda et al. 2010)
Radiation	JMA (2013), Yabu (2013)	JMA (2013), Yabu (2013)	MstranX (Sekiguchi & Nakajima, 2008)	MstranX (Sekiguchi & Nakajima, 2008)
Land and ocean	SiB (JMA, 2013)	SiB (JMA, 2013)	Bucket （Option: 3D ocean model）	MATSIRO (Takata et al. 2003) Slab ocean model
Surface boundary layer	Louis (1982), Miller (1989, Ocean/ Unstable atmosphere)	Louis (1982), Miller (1989, Ocean/ Unstable atmosphere)	Zhang & Anthes (1982) for land surface; Fairall et al. (1996; 2003) for ocean surface	Louis (1979)

(*3): Full-level pressure for surface pressure = 1000 hPa

Geosci. Model Dev. Discuss., doi:10.5194/gmd-2016-184, 2016
Manuscript under review for journal Geosci. Model Dev.
Published: 2 August 2016

Geoscientific Model Development Discussions

Table 5 Computational performance in 12 September 2013, 00:00:00 UTC case

Model	Time step (s)	Number of nodes	Elapse time (sec) (including output of model data)	Node×hours	Execution efficiency (%)
DFSM	200	320	7673	682	4.0
MSSG	17.7	512	16381	2330	15.1
NICAM	30	640	6497	1155	16.5
GSM	400	10	5896	16.4	16.0

Geosci. Model Dev. Discuss., doi:10.5194/gmd-2016-184, 2016
Manuscript under review for journal Geosci. Model Dev.
Published: 2 August 2016

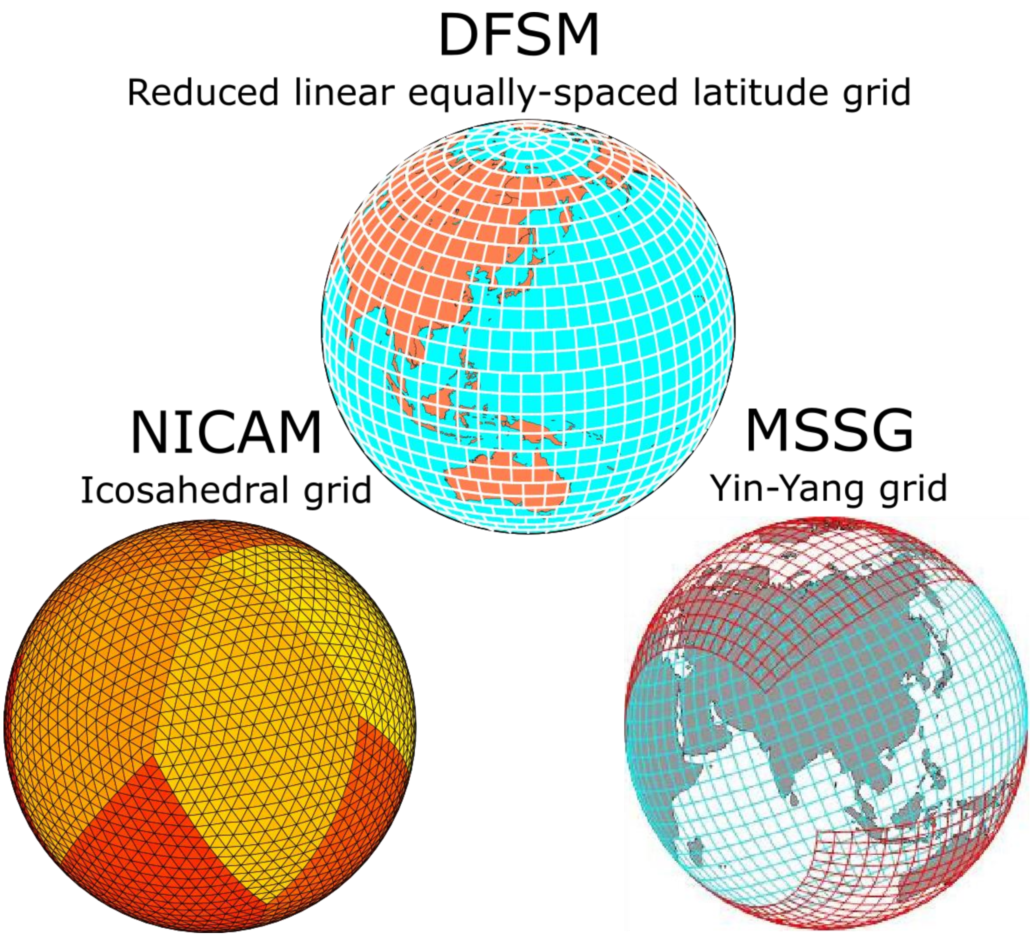

Figure 1: Schematic diagram of horizontal grid structures of three models used in TYMIP-G7

Geosci. Model Dev. Discuss., doi:10.5194/gmd-2016-184, 2016
Manuscript under review for journal Geosci. Model Dev.
Published: 2 August 2016

Geoscientific Model Development Discussions
Open Access

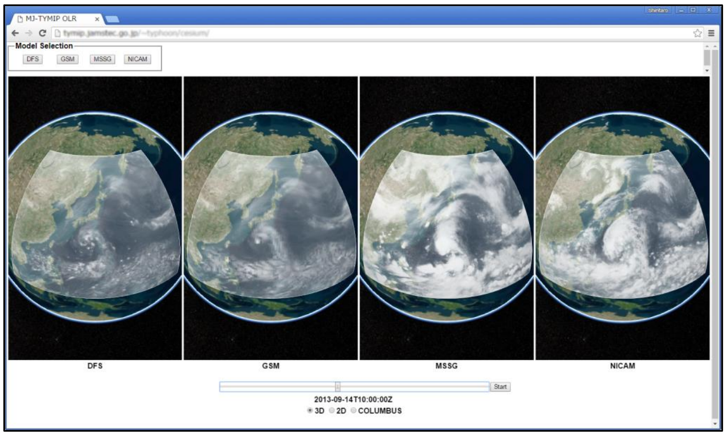

Figure 2: Screen capture of Web application: outgoing longwave radiation at 14 September 2013, 10:00:00 UTC simulated in experiments initialized at 12 September 2013, 06:00:00 UTC.

Geosci. Model Dev. Discuss., doi:10.5194/gmd-2016-184, 2016
Manuscript under review for journal Geosci. Model Dev.
Published: 2 August 2016

Geoscientific Model Development
Discussions
Open Access

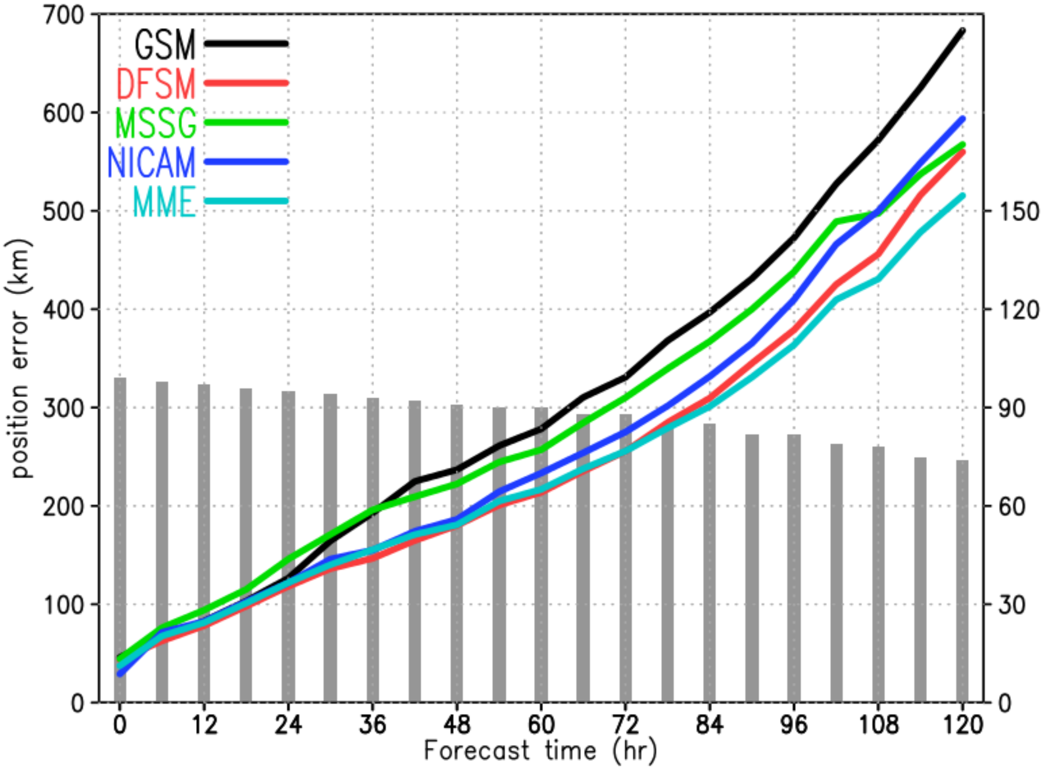

Figure 3 Errors in track prediction for GSM, DFSM, MSSG, NICAM and MME (in second stage). Each grey bar indicates number of samples at each forecast time (right vertical axis).

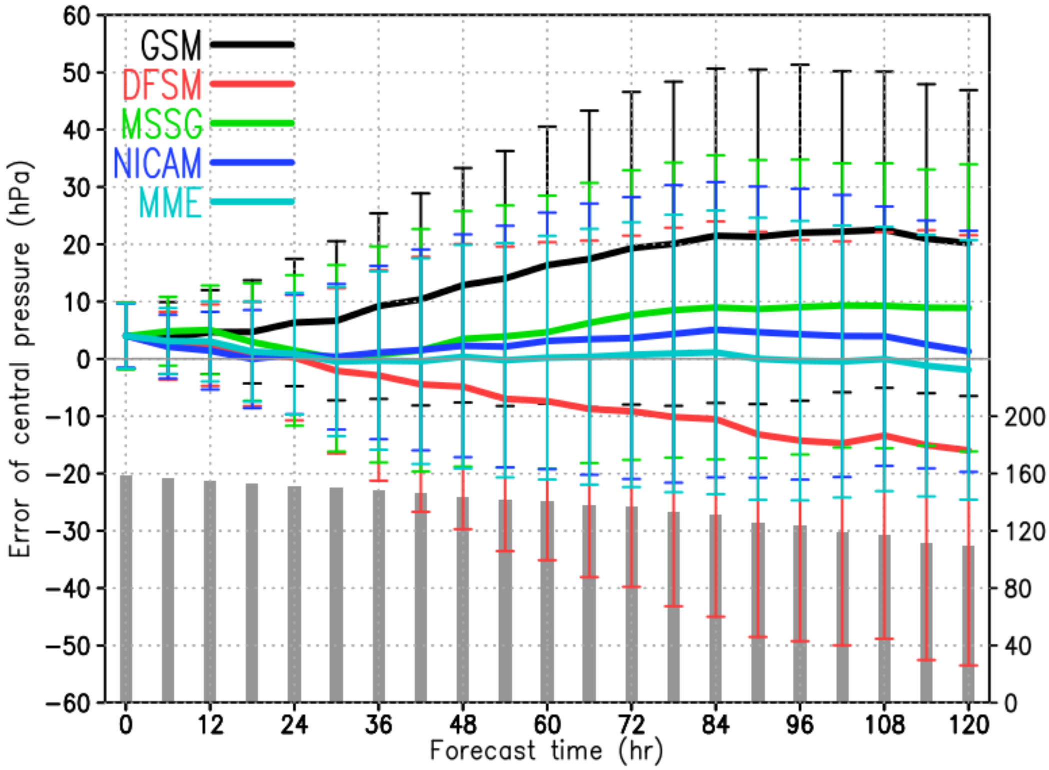

5 **Figure 4 Errors in predictions of central pressure for GSM, DFSM, MSSG, NICAM and MME. Each grey bar indicates number of samples at each forecast time (right vertical axis). Error bars indicate standard deviation of central pressure difference between prediction and JMA best track.**

Geosci. Model Dev. Discuss., doi:10.5194/gmd-2016-184, 2016
Manuscript under review for journal Geosci. Model Dev.
Published: 2 August 2016

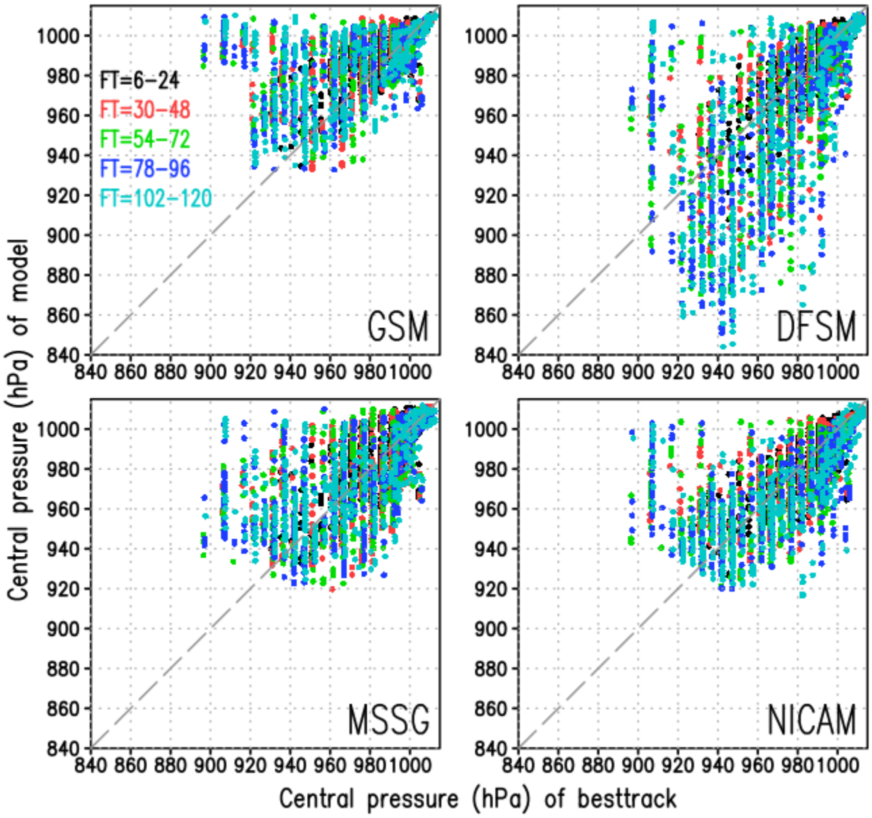

Figure 5 Scatter diagrams of relationship between predicted (y-axis) and best-track (x-axis) central pressures

Geosci. Model Dev. Discuss., doi:10.5194/gmd-2016-184, 2016
Manuscript under review for journal Geosci. Model Dev.
Published: 2 August 2016

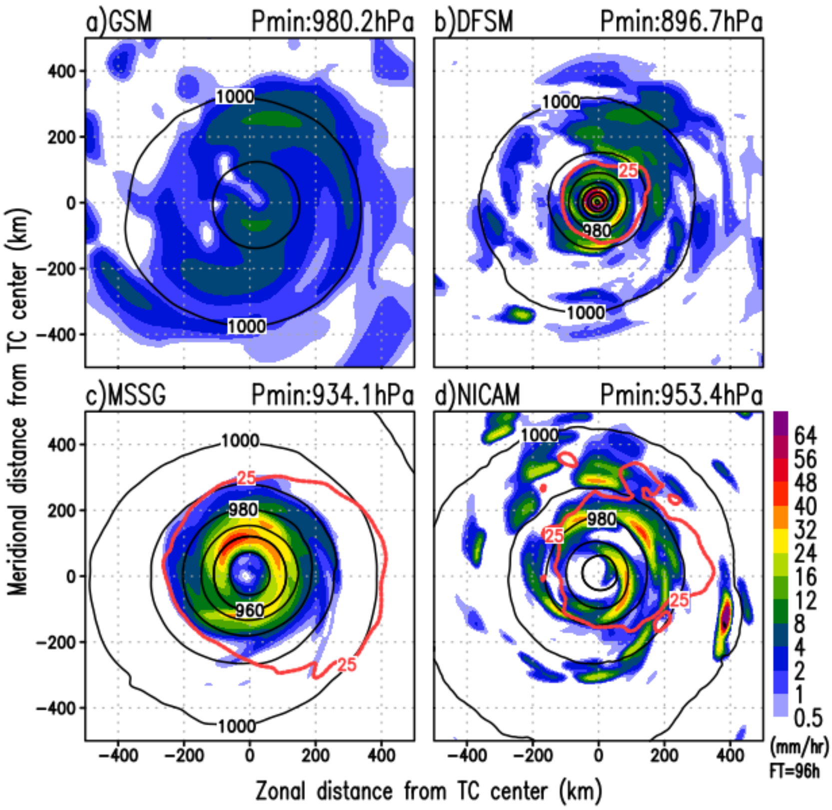

Figure 6 Horizontal distributions of precipitation (colour), sea level pressure (black contour) and wind speed 25 m s^{-1} (red contour) for Typhoon Wipha at FT = 96 h. Labels on horizontal and vertical axes shows zonal and meridional distances from TC centre (km), respectively. Contour intervals of sea level pressure are 10 hPa for > 960 hPa and 20 hPa for < 960 hPa. Plotted area is a 1000-km square and (x, y) = (0, 0) is set to TC centre.

Geosci. Model Dev. Discuss., doi:10.5194/gmd-2016-184, 2016
Manuscript under review for journal Geosci. Model Dev.
Published: 2 August 2016

Geoscientific Model Development Discussions

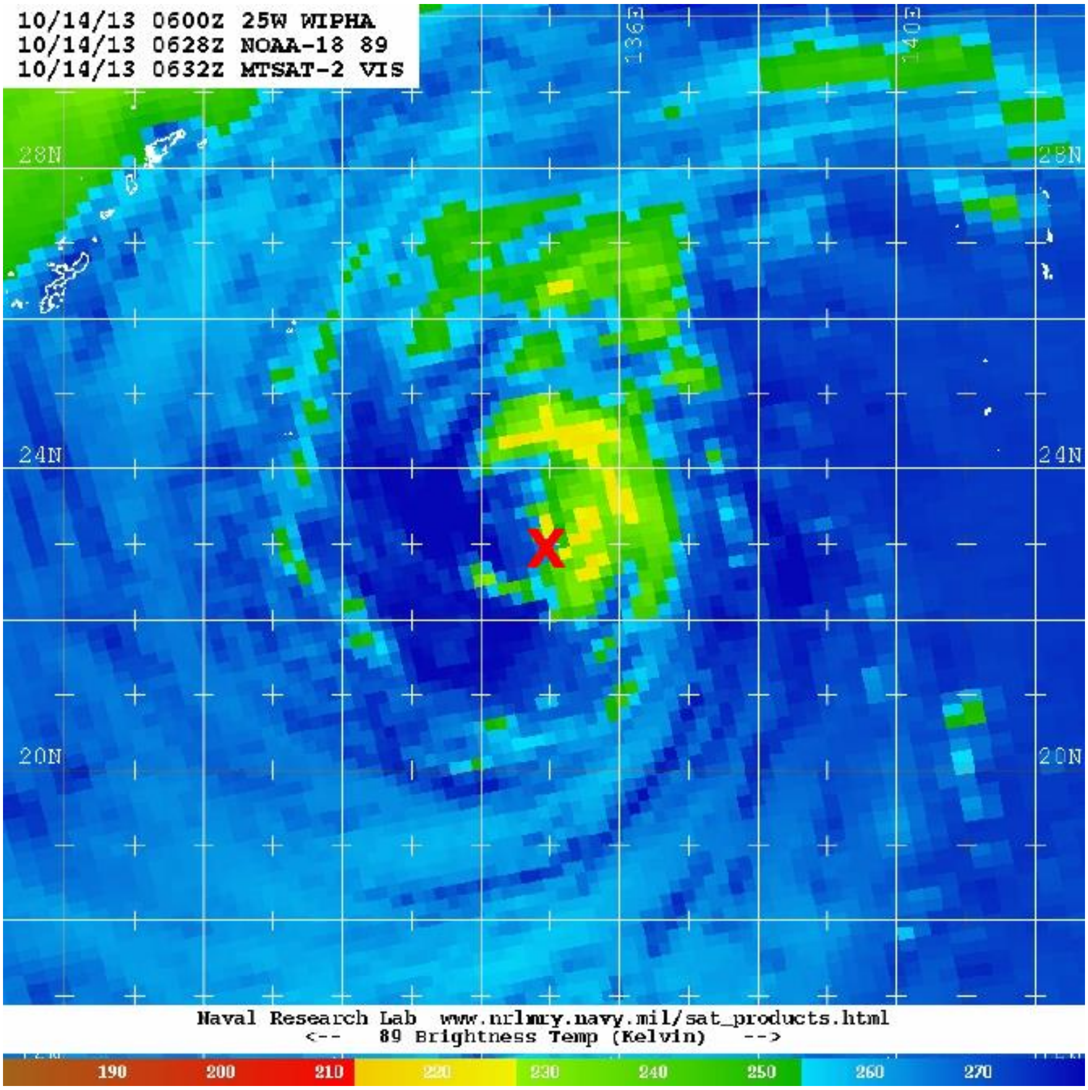

Figure 7 Brightness temperature observed by Advanced Microwave Sounding Unit – A (AMSU-A) channel 89 GHz onboard NOAA-18 at 14 October, 2013 06:28 UTC. (image courtesy of Naval Research Laboratory). Red "X" displays TC Wipha centre.

5

Geosci. Model Dev. Discuss., doi:10.5194/gmd-2016-184, 2016
Manuscript under review for journal Geosci. Model Dev.
Published: 2 August 2016

Geoscientific Model Development Discussions
Open Access

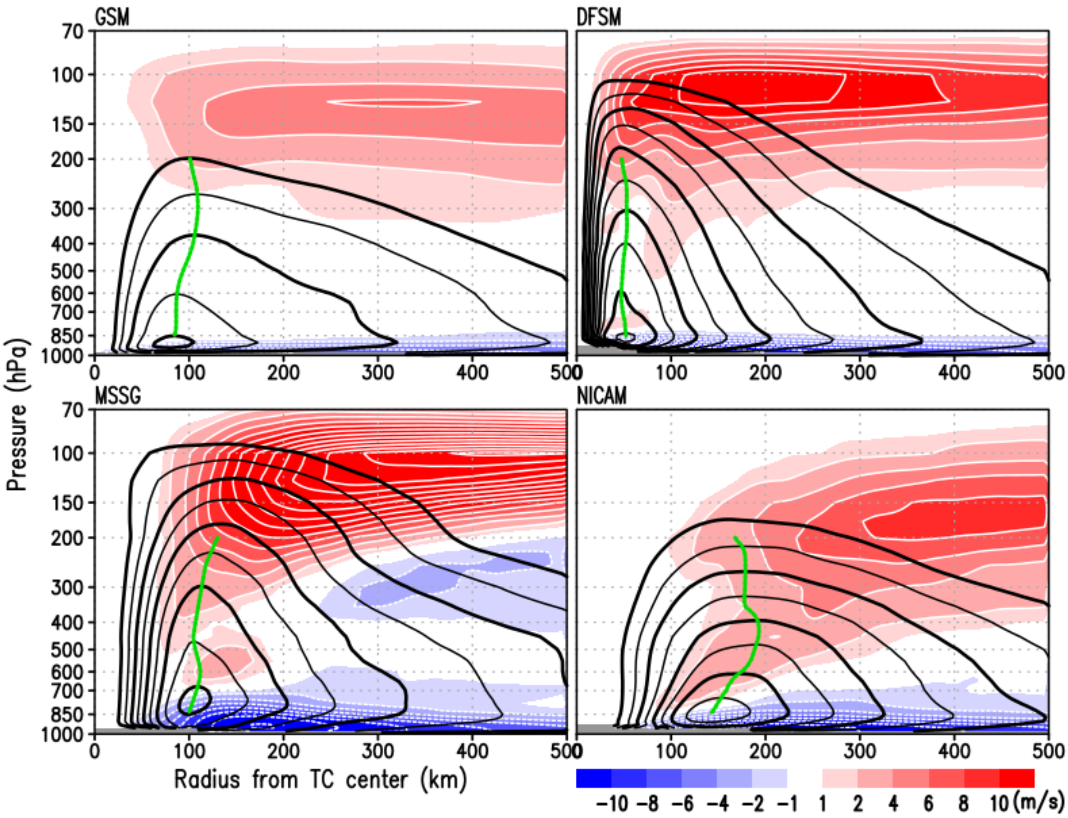

Figure 8 Composite analysis of r-z cross sections of axisymmetric mean radial (shaded) and tangential (contour) wind speeds. Contour intervals are 5 m s^{-1} (values > 15 m s^{-1} are plotted). Green line depicts RMW between 850 and 200 hPa. Grey shading at bottom of each panel is below the surface.

Geosci. Model Dev. Discuss., doi:10.5194/gmd-2016-184, 2016
Manuscript under review for journal Geosci. Model Dev.
Published: 2 August 2016

Geoscientific Model Development
Discussions
Open Access

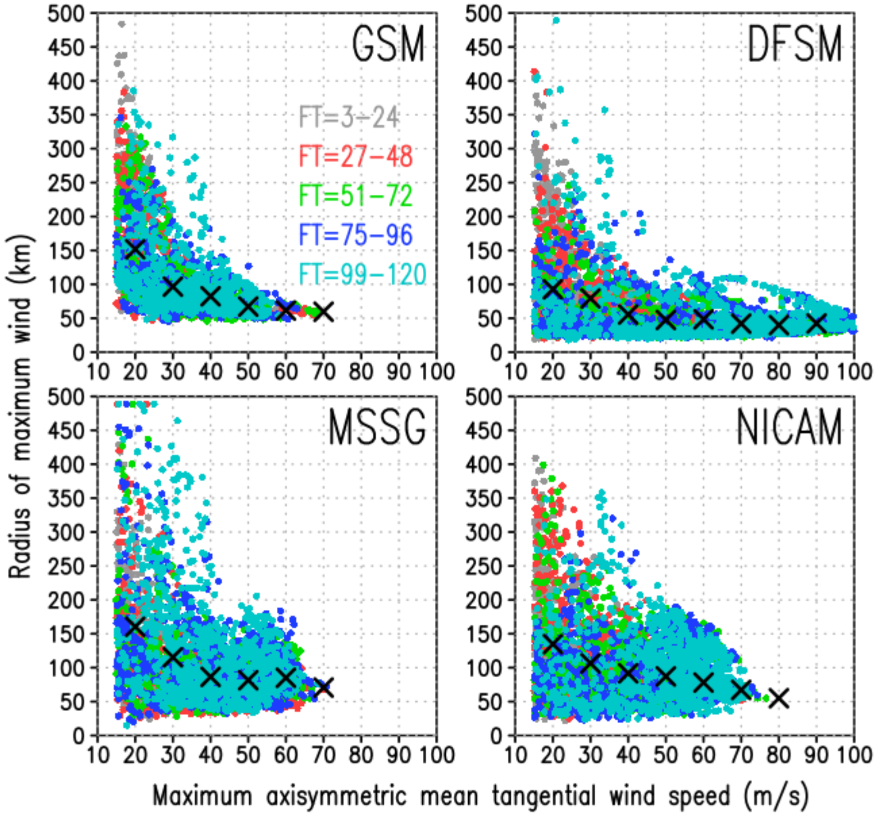

Figure 9 Scatter plot of maximum axisymmetric mean tangential wind speeds (x-axis; m s^{-1}) and radius of maximum wind speeds (RMW, in km). Colours show forecast times (in h) of 3–24 (grey), 27–48 (red), 51–72 (green), 78–96 (blue), and 99–120 (cyan). X marks indicate mean RMW for each intensity (e.g., "20" uses all cases in which intensity is between 15 and 25 m s^{-1})